remote sensing

MDPI

Article

Weather Radars Reveal Environmental Conditions for High Altitude Insect Movement Through the Aerosphere

Samuel Hodges [1,*], Christopher Hassall [2] and Ryan Neely III [3]

[1] School of Earth and Environment, University of Leeds, Leeds LS2 9JT, UK
[2] School of Biology, University of Leeds, Leeds LS2 9JT, UK; c.hassall@leeds.ac.uk
[3] National Centre for Atmospheric Science, Fairbairn House, Leeds LS2 9PH, UK; r.neely@leeds.ac.uk
* Correspondence: sam.jir.hodges@btinternet.com

Abstract: High-flying insects that exploit tropospheric winds can disperse over far greater distances in a single generation than species restricted to below-canopy flight. However, the ecological consequences of such long-range dispersal remain poorly understood. For example, high-altitude dispersal may facilitate more rapid range shifts in these species and reduce their sensitivity to habitat fragmentation, in contrast to low-flying insects that rely more on terrestrial patch networks. Previous studies have primarily used surface-level variables with limited spatial coverage to explore dispersal timing and movement. In this study, we introduce a novel application of niche modelling to insect aeroecology by examining the relationship between a comprehensive set of atmospheric conditions and high-flying insect activity in the troposphere, as detected by weather surveillance radars (WSRs). We reveal correlations between large-scale dispersal events and atmospheric conditions, identifying key variables that influence dispersal behaviour. By incorporating high-altitude atmospheric conditions into niche models, we achieve significantly higher predictive accuracy compared with models based solely on surface-level conditions. Key predictive factors include the proportion of arable land, altitude, temperature, and relative humidity.

Keywords: weather; niche modelling; insects; movement ecology; radar; remote sensing

Citation: Hodges, S.; Hassall, C.; Neely, R., III. Weather Radars Reveal Environmental Conditions for High Altitude Insect Movement Through the Aerosphere. *Remote Sens.* **2024**, *16*, 4388. https://doi.org/10.3390/rs16234388

Academic Editors: Grant Hamilton and Evangeline Corcoran

Received: 15 July 2024
Revised: 29 October 2024
Accepted: 5 November 2024
Published: 24 November 2024

1. Introduction

Insects play a critical and multifaceted role in ecological systems. They serve as vital intermediaries within trophic networks, bridging the gap between producers and large-bodied consumers [1–3]. The role that insects play in resource processing is central to nutrient cycling, facilitating decomposition and subsequent nutrient assimilation [3,4]. Moreover, insects act as keystone species that regulate plant community composition through herbivory and pollination services [1–4]. Due to their wide-ranging involvement in ecological processes, changes in insect population structure or distribution (e.g., range shifts, see Doak and Morris, 2010; Tomiolo and Ward, 2018 [5,6]) can produce impacts that have cascading effects across the entire ecosystem [2,7,8]. Ecosystem change brought about by insects is also not confined to the local population but can impact other nearby populations and habitats through the flows of individuals (and associated nutrients and biomass) among habitats [2,7,8].

The flow of insects and associated nutrients and functions is driven by the capacity for movement, of which flight is a common and highly effective mode. The ability of flying insects to enter the air column and traverse meaningful distances is a significant factor in insect dispersal capabilities and determines the exchange of individuals among habitats. However, there is a wide range of powered flight ability between families of insects with different morphotypes [9–12]. For example, odonates and lepidopterans have been found to be capable of long-distance migrations in a single generation [13–15], and lepidopterans have been shown to carry out directed flight while accounting for crosswinds [16,17].

Smaller, shorter-winged insects like aphids (3.2–4.3 mm, see Bell and Shephard (2024) [18]) and thrips are also found in large numbers in the air column during mass emergence events [18–20], although their mode of flight leaves them highly vulnerable to loss of flight control (aphids fly at up to 0.70 $m \cdot s^{-1}$ in laboratory conditions, see Bell and Shephard (2024) [18]), even under fairly slow windspeeds [21–25].

Regardless of flight ability, when insects fly above the canopy layer, even weak fliers become capable of travelling great distances by exploiting the wind. In contrast, dispersal through the terrestrial environment is limited to powered flight alone. Dispersal at higher altitudes is underexplored and rarely included by range shift and habitat connectivity studies, which have been used as the basis for future conservation and pest management policy [26–30]. For example, it is unclear to what extent tropospheric winds contribute to dispersal, how wind-assisted flight contributes to the functional connectivity of habitats that might be considered unconnected under conventional models of dispersal, and the taxonomic breadth of species exploiting high-altitude dispersal routes. Thus, the consequences of high-altitude dispersal remain unexplored, but such a phenomenon raises the possibility of complex responses to habitat fragmentation and resulting climate change-induced range shifts [31–34]. As high-flying insects (active at heights above the ground >100 m) could be capable of continuing dispersal or migration between increasingly isolated terrestrial patches, using the aerosphere as a corridor, the functional connectivity of habitat patches could be greater than for below-canopy fliers [33,35–37]. However, the ecological modelling literature has largely neglected the aerosphere as a distinct habitat due to traditionally constrained observational capabilities, leading to the assumption that atmospheric interactions constitute only a brief phase in organism life histories [38,39]. Therefore, there is a need to recognise the ecological importance of 'flight niches' in insect dispersal ecology, a concept already applied to a few pioneering avian studies [40,41].

One key limitation to studying flight niches is the difficulty of observing organisms at high altitudes. Previous aeroecological studies have addressed this challenge chiefly through vertical-looking radars (VLRs) and traditional field sampling. VLRs have been able to observe the stratification of insect activity into layers at given altitudes [16,42–44], as well as favouring of specific windspeeds (the flight boundary layer concept) and directions during flight [15,24,42,45]. However, VLR studies have been restricted to studying the vertical distribution of insects at single sites, over short timescales [42,46,47]. Field studies, on the other hand, have provided richer diversity and population data on flying insects over wide spatial scales, but with poor spatial resolution, and they are typically restricted to low-altitude observation [10,15].

Compared with VLR and field studies, weather surveillance radars (WSRs) like the NCAS mobile X-band [48] can provide greater coverage of insect aerial presence (the X-band typically detects insects up to a ~30 km horizontal radius around the radar, and from 100 to 3000 m altitude above sea level) and over annual to decadal timescales [9,13,49–51]. Unlike VLRs, which detect individual scatterers [52] in a thin, vertically pointing beam, WSRs have the advantage of a wide beam that scans along the horizontal as well as the vertical, allowing applications such as the estimation of the spread of insect outbreaks [9]. A further advantage to using WSR data is that a wide range of devices are already deployed globally as part of national meteorological services, several of which make their data accessible to academics [50,53]. Observations from WSRs have been used to demonstrate the weather-dependence of seasonality in insect and winged vertebrate mass emergences over large spatial scales [41,53–55]. Thus, WSRs represent an underexplored opportunity to correlate high-altitude insect presence with meteorology to better our understanding of long-distance insect dispersal and aerial habitat connectivity [36,56–59].

Studies based on observations from WSRs and VLRs [38,60–62] have shown that passive dispersal models (e.g., the Lagrangian movement) do not offer an adequate description of insect flight behaviour, which appears to contain elements of both active and passive dispersal (see [63,64] for a comparison of active/passive dispersal concepts). Further, insects appear to prefer certain atmospheric conditions for flight, as shown in VLR studies.

Aeroecological studies have previously used the relationship between animal presence and environmental conditions to characterise active dispersal behaviour. For example, Wang et al. (2023) [65] draw on several documented behavioural responses to environmental thresholds, which they use to inform their dispersal model of fall armyworm [66,67]. Aralimarad et al. (2011) [42] also used correlations with windspeed direction to explain common orientation and clustering of individual insects around specific altitudes. However, establishing consistent correlations requires significant research efforts per species, which limits the generalisability of this approach [28,65,68,69]. Furthermore, the atmospheric variables that have been used in previous ecological studies are often restricted, with the majority focusing on more easily measured variables with an obvious biological impact, such as temperature and relative humidity [21,70–72]. These variables are also generally measured at the surface level or under controlled conditions, where vertical variability and multivariate collinearity are difficult to observe.

Here, we combine WSR-based observations of insects in flight with contemporaneous three-dimensional, high-resolution atmospheric data to characterise presence–environment correlations using environmental niche modelling (ENM). We demonstrate our radar-based niche modelling approach during the deployment of an X-band radar system over a year. We test the hypothesis that the incorporation of high-altitude meteorological variables enhances our ability to predict insect presence compared with models containing only surface-level predictors. If supported, these findings would indicate that insects are monitoring and responding to their environment after take-off to ensure they remain in suitable conditions for continued flight (active dispersal). We further investigate which atmospheric variables are the primary correlates of aerial insect activity within the region and time of our study and contrast the relative importance of surface variables with high-altitude variables. Identification of key predictor variables would allow us to make mechanistic inferences about the link between environmental conditions and the behavioural strategies of flying insects. Finally, we illustrate the effect of the dynamic atmosphere on the spatial distribution of suitable tropospheric habitats over time.

2. Materials and Methods

2.1. Data Used in This Study

2.1.1. The NXPol-1 Weather Surveillance Radar

WSR observations were sourced from the NCAS (National Centre for Atmospheric Science) mobile dual-polarisation Doppler X-band WSR (NXPol-1, Meteor 50DX model, made by Selex-Gematronik, Neuss, Germany; [48]), which was deployed at the NERC Facility for Atmospheric Radar Research (NFARR) at Chilbolton (near Hampshire in the United Kingdom; 51.14N, −1.44E; [48]). The deployment took place from November 2016 to June 2018.

NXPol-1 was deployed on a scanning regime of 10 elevations over 0.5 to 20 degrees. A complete scanning regime took approximately 5 min, with a single 360-degree scan at one elevation taking close to 30 s. NXPol-1 collected observation data from 75 m to 150 km in range in 150 m bins, at an azimuthal resolution of 1 degree. The WSR data had also been pre-filtered based on a signal-to-noise ratio to remove non-significant echoes. This scanning regime was repeated over the course of every active day during the deployment. We made an initial selection of hourly data from the 1 January to the 31 December 2017.

2.1.2. The ECMWF Operational Forecast Model

For this study, we chose to represent the atmospheric environment with data sourced from the European Centre for Medium Range Weather Forecasting (ECMWF) MARS operational archive (© 2017 European Centre for Medium-Range Weather Forecasts (ECMWF), www.ecmwf.int (https://apps.ecmwf.int/datasets/licences/general/, accessed 26 November 2023), CC BY 4.0, ECMWF does not accept any liability whatsoever for any error or omission in the data, their availability, or for any loss or damage arising from

their use). The ECMWF Operational Forecast provides high spatial and temporal resolution data, with a wide range of surface and tropospheric variables [73]. The data were downloaded at a resolution of 0.07 by 0.07 degrees (~4 × 8 km, longitude x latitude) across a bounding box of 49°–60°N and 12°W–5°E. Atmospheric variables were downloaded on pressure levels 1000, 900, 800, and 700 hPa (roughly corresponding to 0, 1000, 2000, and 3000 m altitude above sea level) at an hourly interval for a 0–11 h range for forecasts started at 00:00 and 12:00 h (the initial conditions, equivalent to an analysis step; see ECMWF (2023) [73]) for the entire year of 2017. We also downloaded surface variables on the same grid, temporal resolution, and time range. The ECMWF operational forecast data effectively represents instantaneous values taken at every hour of the simulation [73], so we were able to consider the closest radar file in time as near-simultaneously observed with the conditions of the atmosphere.

The ECMWF operational forecast offers variables that vary over pressure levels (altitude) and 'Surface' variables that are independent of pressure levels, either because they affect the entire air column or are modelled to a fixed altitude (e.g., 2 m, 10 m). To test our hypothesis that atmospheric variability within the air column is a better predictor than surface-level measurements alone, we downloaded variables from both the pressure levels and surface datasets. We divided them into 'Aerial' (pressure levels) and 'Terrestrial' (surface) categories for comparison in later niche modelling; see Table 1 for a complete list of the variables we selected.

Table 1. Categorised list of ECMWF atmospheric variables and CEH land cover types used in this study. A description of all variables (except altitude band and time) in the ECMWF forecast model can be found at https://codes.ecmwf.int/grib/param-db/, accessed 26 November 2023 [73]. The land cover types are described in detail at https://catalogue.ceh.ac.uk/documents/f6f86b1a-af6d-4ed8-85af-21ee97ec5333, accessed 26 November 2023, and in Morton et al. (2020) [74].

Variable Category	Variable Type	Variable Full Name	Units
Aerial (Pressure Levels)	Wind	Zonal Wind	m s^{-1}
		Meridional Wind	m s^{-1}
		Vertical Velocity	Pa s^{-1}
	Stability and Flow	Divergence	s^{-1}
		Relative Vorticity	s^{-1}
		Potential Vorticity	K° m^{-2} kg^{-1} s^{-1}
	Temperature	Temperature	C°
	Precipitation	Relative Humidity	%
	Geometry	Altitude Band	m (±500 m)
		Time	Hours
Terrestrial (Surface)	Wind	10 m U-component of Wind	m s^{-1}
		10 m V-component of Wind	m s^{-1}
		Instantaneous 10 m Wind Gust	m s^{-1}
	Temperature	2 m Temperature	C°
		Skin Temperature	C°
	Precipitation	Convective Rain Rate	Kg m^{-2} s^{-1}
		Large Scale Rain Rate	Kg m^{-2} s^{-1}
	Geometry	Time	Hours
	Land Cover Type	Broadleaf Woodland	%
		Coniferous Woodland	%
		Arable	%
		Grassland	%
		Urban–Suburban	%

The seven 'Terrestrial' variables were selected to include temperature and wind conditions at ground level, to act as a control against vertical variability (Table 1). Surface-level conditions have been frequently associated with the timing of insect mass dispersal events, such as soil temperature and humidity in the seasonal emergences of winged *Lasius niger* [71,75,76], and wind direction in dragonflies [15].

2.1.3. Centre for Ecology and Hydrology Land Cover Maps

In addition to the above atmospheric data, we included the proportion of land cover types inside the ECMWF grid cells. The Land Cover Data used in this study is owned by UK Centre for Ecology & Hydrology (© Database Right/Copyright UKCEH). Knop et al. (2023) [77] recently conducted an analysis that demonstrated a correlation between aerial insect abundance and the type of habitat at the surface of the atmospheric column, where the insects were observed. To test whether this produced similar effects on the spatial extent of aerial insect presence, we included a list of these habitat types from the Centre of Ecology and Hydrology (CEH) land cover maps [74] in the terrestrial variables we supplied for niche modelling (Table 1).

The CEH land cover map was downloaded for the year of 2017 on a 1 km resolution. The CEH maps are provided on the British National Grid (EPSG: 27700; [74]), so we reprojected the data onto longitude–latitude coordinates at a resolution of 0.04 × 0.04 degrees (approximately similar to the ECMWF grid, 0.07 × 0.07) using QGIS [78]. We transformed the data from the categorical land cover types to percentages of land cover contained in the new grid cells. Then, we averaged these percentages of land cover per ECMWF grid cell, to find the proportions of land cover type at surface level. As the Chilbolton study site was unlikely to contain certain habitat types in abundance, we limited our selection of land cover types to broadleaf and coniferous woodland, arable land, grassland and urban–suburban (built-up areas); see Morton et al. (2020) [74] for the full list of land cover types.

2.2. Methodology

2.2.1. Overview

To address these research aims, we have developed a methodology that makes use of paired observations of insect aerial activity derived from WSR observations and archived data describing the atmospheric and other environmental conditions. In this and the following sections, we summarise the approach we have used to create this paired data (presence-absence-environment tables) and subsequent ENM analysis of their covariance. The data analysis and storage of this project used JASMIN, the UK collaborative data analysis facility.

The first step was to acquire WSR and atmospheric data. WSR observations had to be sourced from a dual-polarisation WSR system that recorded equivalent reflectivity factor in the horizontal and vertical (Z_H/Z_V), differential reflectivity (Z_{DR}), and correlation coefficient (ρ_{HV}) (Figure 1, Section 2.1.1). Here, we used a signal-to-noise ratio filtered radar returns from the NCAS NXPol-1 X-band radar system [48]. Atmospheric data had to cover as much of the WSR's spatial and temporal range and resolution as possible. We used weather forecast models from the ECMWF Integrated Forecasting System (IFS) as a source (Figure 1, Section 2.1.2). Weather forecasts were favoured over reanalysis as IFS reanalysis is limited to 6 h intervals. We rejected the hourly reanalysis, ERA5, due to poor spatial resolution (0.25° × 0.25°) compared with IFS forecasts (0.07° × 0.07°). Land cover data were included to test for the effect of habitat types that might have acted as sources of or destinations for insects moving through the air column. We sourced land cover data from the UK Centre for Ecology and Hydrology UK land cover maps (see Section 2.1.3, CEH).

The second step was to classify and filter the radar data so only insect presence–absence observations remained. The filtering procedure had to exclude meteorological scatterer and correspond to known patterns of insect signatures in WSR observations. The

filtering steps produced a spatiotemporal record of true/false presence–absence for a defined biological scatterer class (in the case of this study, Insecta) on the spherical coordinate system of the radar, defined by its range gates and scanning regime (which defined the azimuthal resolution and elevation angles).

Next, the spherical presence–absence data were paired with atmospheric data by gridding them to the geographic coordinate system used by the atmospheric data (Figure 1, Section 2.2.3). The presence–absence data points were treated as single voxels (a 'voxel' being equivalent to a radar range bin in 3D space), representing the centroid of their spherical coordinate voxel. The voxels were then counted per atmospheric grid cell. Then, we assigned each cell a single value dependent upon whether it contained absences, presences, or neither (see Section 2.2.3). The gridding process was performed for each timestep of atmospheric data to get paired presence–absence and environment observations as close in time as possible. Gridding resulted in a presence–absence–environment table including all the observations of true presence and true absence with the corresponding states of the environmental variables of interest.

The presence–absence–environment tables need to be reduced due to the high resolutions of the radar and atmospheric data. High resolution and range (compared to biological field surveys) result in a large number of observations even after filtering, so the tables are often too big to analyse efficiently with R implementations of niche modelling (see Thuiller et al. (2023) [79] for a package list) and contain a large number of redundant observations (identical data). Therefore, our next step was to reduce the number of rows in the table through random subsampling or another equivalent method (Figure 1, Section 2.2.3). We implemented a constrained random subsampling process, which preserved the proportion of presences to absences and the distribution of values for the environment variables. In this way, we subsampled the data to much smaller tables, while limiting introduced bias from random sampling.

The final step was to carry out niche modelling on the subsampled presence–absence–environment tables (Figure 1, Section 2.2.4). We implemented niche modelling using the 'biomod2' package, using the 'tree', 'glm', 'rpart', and 'randomForest' R packages [79]. ENMs produced several types of assessment statistics to investigate the quality of the model and the roles of predictor variables. In this study, we addressed our research aims by analysing model assessment statistics under different variable selections (surface level, high-altitude, and both combined, see Section 2.2.4), followed by a comparison of variable importance metric, and then the response curves of the most important variables (Figure 1, Section 2.2.4). These models could then be projected onto gridded environment data to picture how the atmospheric data could influence spatial distributions of flying organisms (Figure 1, Section 2.2.4).

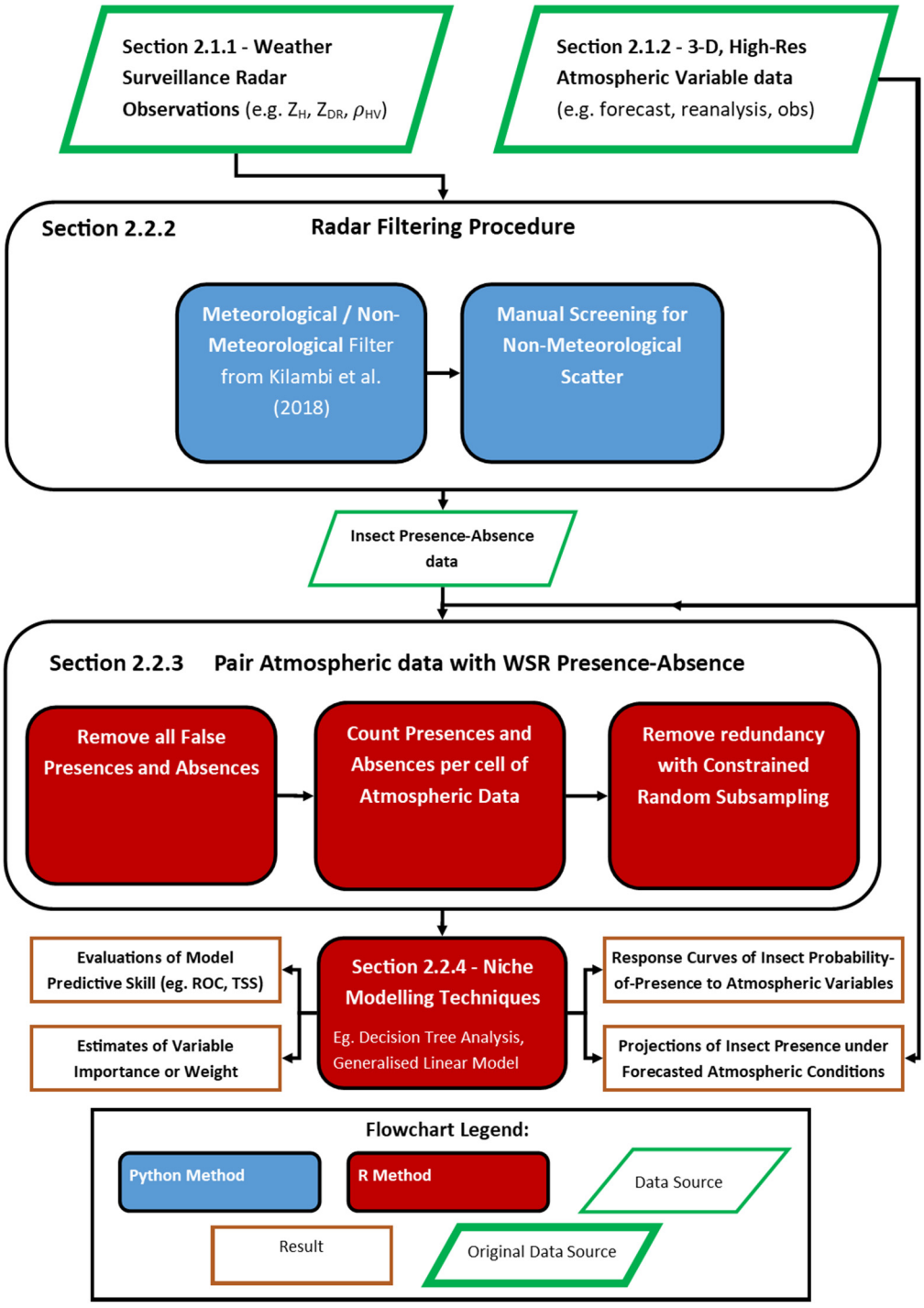

Figure 1. A high-level, generalised overview of our WSR-ENM procedure. The procedure can be considered to comprise two principal stages, radar filtering into insect presence–absence data and the pairing of 3D gridded atmospheric data with insect presence–absence [80]. This procedure produces Species with Data tables which can be used with a range of niche modelling approaches.

2.2.2. WSR Filtering Procedure

We first selected processed WSR data (see Section 2.1.1) from the recordings to create an hourly resolution dataset, spanning 2017 from the 1 January to the 31 December. All radar voxels in each of these files were then transformed from a list of radar measurements to a classification of presence or absence under the following procedure.

First, we used the 95% confidence thresholds reported by Kilambi et al. (2018) [80] for classifying radar signals as meteorological scatter and non-meteorological scatter

(Figure 2a,b). These thresholds were based on a maximum threshold for reflectivity (Z_H < 35 dBZ) and the depolarisation ratio (DR < −12), which was calculated from the linear scale differential reflectivity (Z_{dr}) and correlation coefficient (ρ_{HV}) using Equation (1) (reproduced from Kilambi et al., 2018 [80]).

$$DR = \frac{Z_{dr} + 1 - 2Z_{dr}^{\frac{1}{2}}\rho_{HV}}{Z_{dr} + 1 + 2Z_{dr}^{\frac{1}{2}}\rho_{HV}} \quad (1)$$

After this classification was applied to the radar voxels, we removed all isolated voxels of non-meteorological scatter, using the despeckling filter provided in the Py-ART Python package. This was applied directly to the classified data, using a threshold of 0.5 (where a non-meteorological voxel is represented as 1, see Table 2) and a group size of 30 [81]. Beam blockages were manually removed within sets of predefined azimuths (54–65°, 82–91°, 128–155°, 175–185°), and ground clutter was removed by excluding voxels from elevations below 2°. Finally, we manually filtered the data of extraneous events that could be misidentified as insect scatter. This included melting layers, sun spikes, interference from other radio sources, chaff from aircraft over the site, and ice-bearing clouds. Unfortunately, as there is no dependable method to remove reflectivity caused by birds from X-band radar scans, we have to admit the possibility of contamination. The outcome of our filtering was a collection of clear-air days containing spatially congruent, non-meteorological scatter, which bloomed from the centre of the radar in accordance with diurnal cycles. An example plan positional indicator (PPI) plot is shown in Figure 2, and we further provide a video overview of all radar moments filtered from over our study period in the Supplementary Materials.

Table 2. Final designations of signal types in our WSR-ENM procedure, the corresponding data code, and abbreviated rules for determining type. Az—azimuth, El—elevation, DR—depolarisation ratio, Z_H—horizontal reflectivity, SNR—signal-to-noise ratio, NA—not available, '|'—or, '&'—and.

Signal Type	Presence/Absence Code	Determinants
Non-Meteorological (TP)	1	DR > −12 & Z_H < 35 & SNR > 0.5
No Signal (TA)	0	Z_H = NA | SNR < 0.5
Weather (FA)	−1	DR < −12 | Z_H > 35 | SNR > 0.5
Beam Blockage (FA)	−2	54° < Az < 65° | 82° < Az < 91° | 128° < Az < 155° | 175° < Az <185° | El < 2°
Indeterminate Scatter (FA)	−3	Z_H!= NA & Z_V = NA

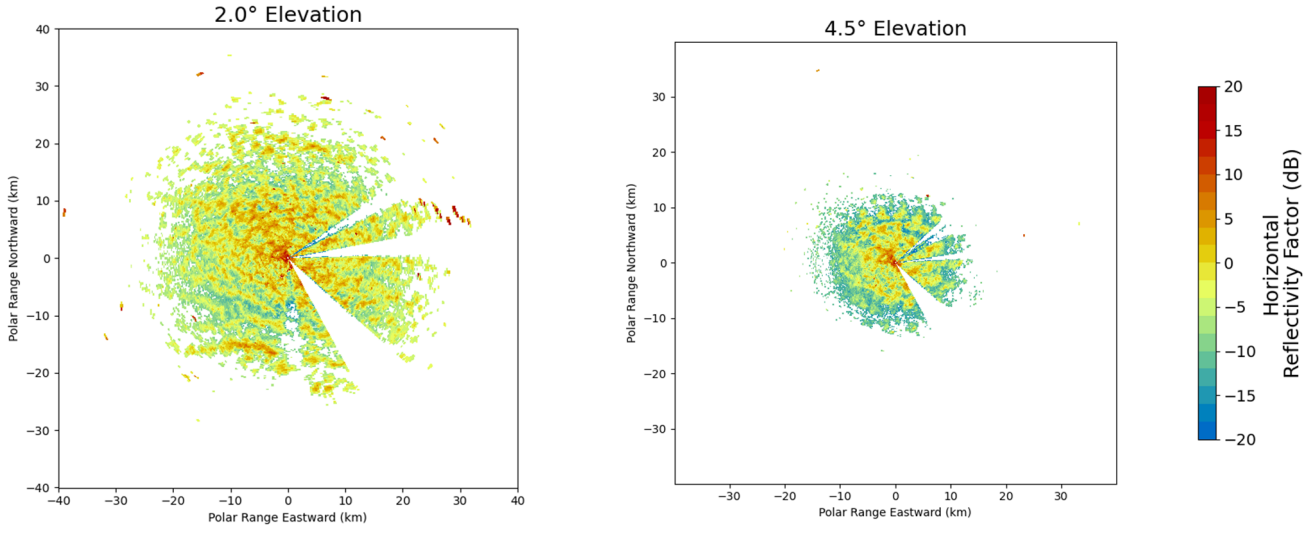

(**a**) (**b**)

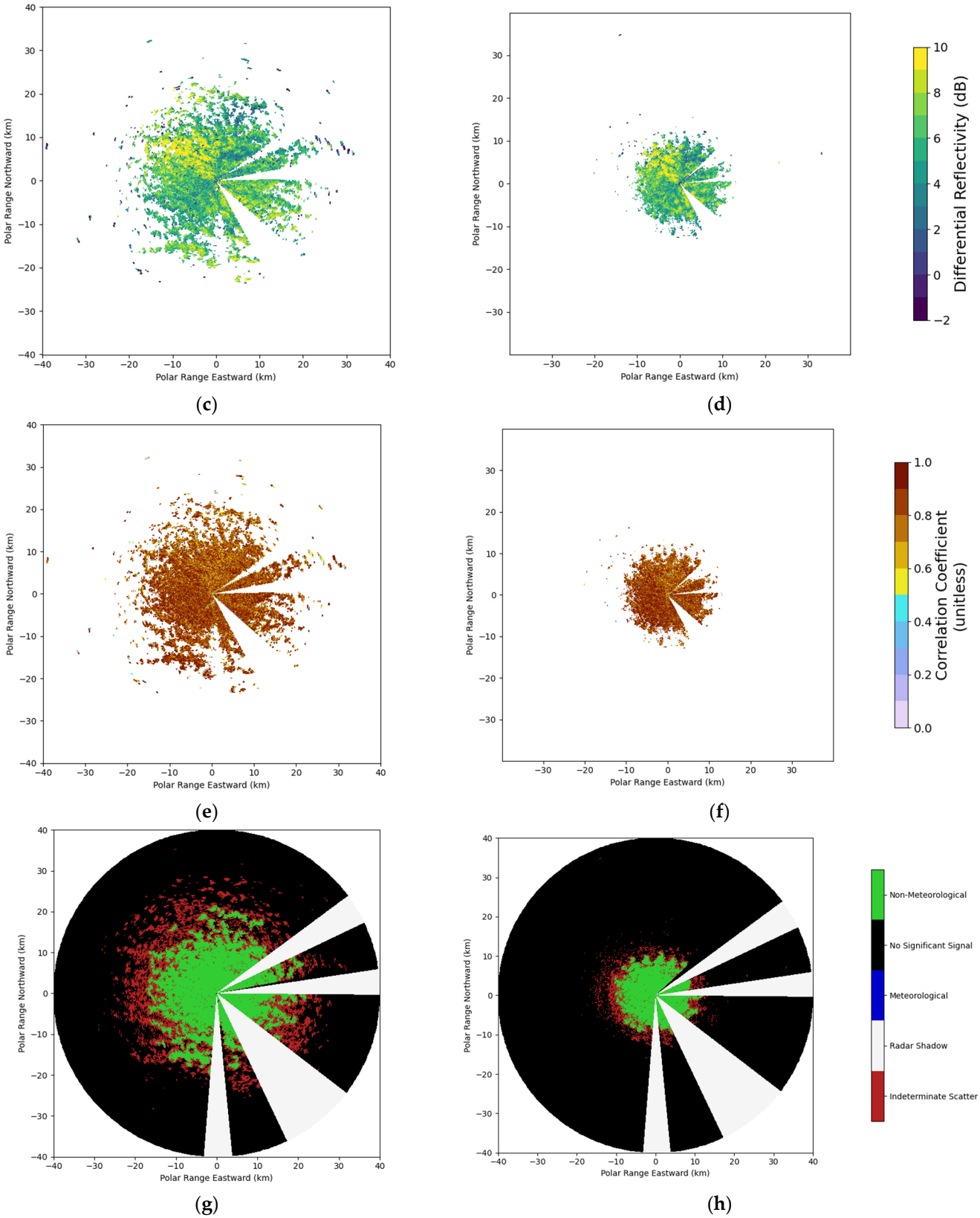

Figure 2. Outcome of radar filtering applied to NXPol-1 observations (Section 2.1.1) on 10 May 2017 at ~12:00, demonstrated with plan position indicator (PPI) plots at 2.0° (**a**,**c**,**e**,**g**) and 4.5° elevation (**b**,**d**,**f**,**h**) in the radar antenna. See Table 2 for the list of classification rules per signal type. See Figure 1 of Lukach et al., (2022) [82] for a visual depiction of a PPI in real space. (**a**,**b**) Z_H. (**c**,**d**) Z_{DR}. (**e**,**f**) ρ_{HV}. (**g**,**h**). Classifications based on DR (Table 2) (Kilambi et al., 2018) [80]. 'Indeterminate' scatter

beyond the range of insect presence is due to a lack of Z_V and consequently Z_{dr}, resulting from attenuation in the vertical polarisation, which prevents classification by DR.

2.2.3. Pairing of WSR and Atmospheric Data

WSR and atmospheric data were paired using a simple grid-based approach. We used the longitude latitude grid from the atmospheric data to partition the radar voxels (centroids) into raster grid cells. We then counted the number of true presences and true absences (Insects, No Signal; Table 2) per grid cell. Based on the counts of true presence–absence, we then gave each grid cell a single classification: where any true presence data were found, the cell was classified as 'present', regardless of the number of true absences recorded (Table 3). Where no presence data were found, but there were true absences, the grid cell was classified as 'absent' (Table 3). Where no presence or absence data were found (i.e., the cell was outside the radar's effective range or only contained false presences/absences), the cell was classified as 'NA' (Table 3).

Table 3. Designations of presence or absence for ECMWF PA tables, corresponding data code, and abbreviated rules for each type.

Raster Box Designation	Presence/Absence Code	Determinants
True Presence (TP)	1	TP count > 0
True Absence (TA)	0	TP count = 0 & TA count > 0
No Data	NA	TP count = 0 & TA count = 0

We gridded the WSR data to the atmospheric grid. However, there may still be data redundancy (repetitive presence–environment observations) to consider when employing datasets with extensive spatial and temporal range and resolution (e.g., for our selection of data, this resulted in ~24 h × 31 days × 12 months × 1600 cells = ~14.2 million table rows). To reduce redundancy, we used a random subsampling approach to reduce the presence–absence table length by a set of three pre-determined fractions, which we refer to as subsampling factors. The method randomly subsampled presences and absences independently to preserve their proportions in the new table for a user-defined number of iterations (n = 100 in this study). After random subsampling, we selected the table that was the closest fit to the distributions of the atmospheric variables in the original table, based on a least-squares difference between quartile values (See Supplementary Materials for a complete description of this method). To check whether our random subsampling method significantly affected later niche modelling, here we used subsampling factors of 0.01, 0.005, and 0.001.

2.2.4. Niche Modelling with Biomod2

We organised the experimental design for our niche modelling using the biomod2 R package [79]. We selected four widely used algorithms from biomod2 to use in niche modelling to test whether the model assessment statistics (see following paragraph) were influenced by the choice of algorithm, thus inappropriately biasing our ecological interpretations. We selected modelling algorithms to represent two simple implementations of the decision tree family of niche models, as well as the generalised linear model family, and further included a complex algorithm from the decision tree family to allow for a range of species response curve relationships (e.g., thresholds, splines, gradients). These algorithms included Classification Tree Analysis (CTA), Random Forest (RF), and the Generalised Linear Model (GLM). All three algorithms were applied with 100 replications to each subsampled presence–absence–environment table, per selection of environment variables (Aerial, Terrestrial, Aerial and Terrestrial; see Table 1). We therefore produced niche models under three different treatment groups—model algorithm, subsampling factor, and variable types. The model algorithm and subsampling factor treatment groups both served to detect bias in the models resulting from our analytical process, whereas

assessment of the effect of the variable types included was used to answer our primary and secondary science questions. We did not alter any other settings from their defaults in biomod2.

Biomod2 includes a range of model assessment statistics. We chose to use the area under the curve for Receiver Operator Curve (ROC) and True Skill Statistic (TSS) to assess model accuracy, which we used to answer our primary science question by conducting a statistical analysis of these metrics across our three treatment groups, via an analysis of variance (ANOVA). We included TSS alongside ROC as, although ROC is the more traditional metric, it has faced criticism, with TSS being proposed as a more reliable alternative [83–85]. The ANOVA, coupled with a Tukey HSD post hoc test, revealed the treatments associated with the highest accuracy per group and the relative contribution of each treatment group to model predictive skill. We also assessed variable importance—the relative contribution of each variable to model predictions—using biomod2's variable importance metric.

The variable importance metric was based on the response in predicted probability of presence, as the variable of interest was allowed to vary. The variable's values were then 'shuffled' with their spatial coordinates to randomise the variable's spatial distribution. The new values were then fed back into the niche model to obtain a new response value. The response from this random spread was then tested using Pearson's correlation against the original response in probability of presence, using the true data. The resulting Pearson's correlation coefficient was subtracted from 1 to give the variable importance value. Therefore, the more the predictions changed due to spatial randomisation, the higher the variable's importance in the model. The whole process was carried out for a set number of repetitions by the user, with another variable selected randomly for comparison each time (See Thuiller et al. (2023) [79] for more details). Biomod2's variable importance statistic was used to answer our second science question by using a similar ANOVA procedure to the one described for ROC and TSS.

We also produced response curves for variables scoring highly in importance to identify critical limits of presence probability. Finally, we created a simple spatial projection using the GLM onto four days from our dataset, chosen to provide a range in seasonal meteorology. The days chosen were 17 February 2017, 17 April 2017, 17 July 2017, and 17 September 2017. We used these projections in conjunction with our response curve plots for a speculative analysis of the mechanisms influencing insect flight.

3. Results

After we applied our radar filtering procedure to the radar returns from NXPol-1 (Figure 2), we found that insect aerial activity detected across the radar range was highly variable by season in 2017 (Figure 3). While some background activity remained over autumn (particularly October), most activity took place from April to August (on average, at least 1500 forecast grid cells registered presence at midday, Figure 3), with July proving to be the most active month. Insect activity was also observed to be highly diurnal, the majority taking place between 0800 and 1700 (UTC). The diurnal cycle of activity was largely preserved between months. However, activity appeared to be prolonged in June over the morning and evening (Figure 3).

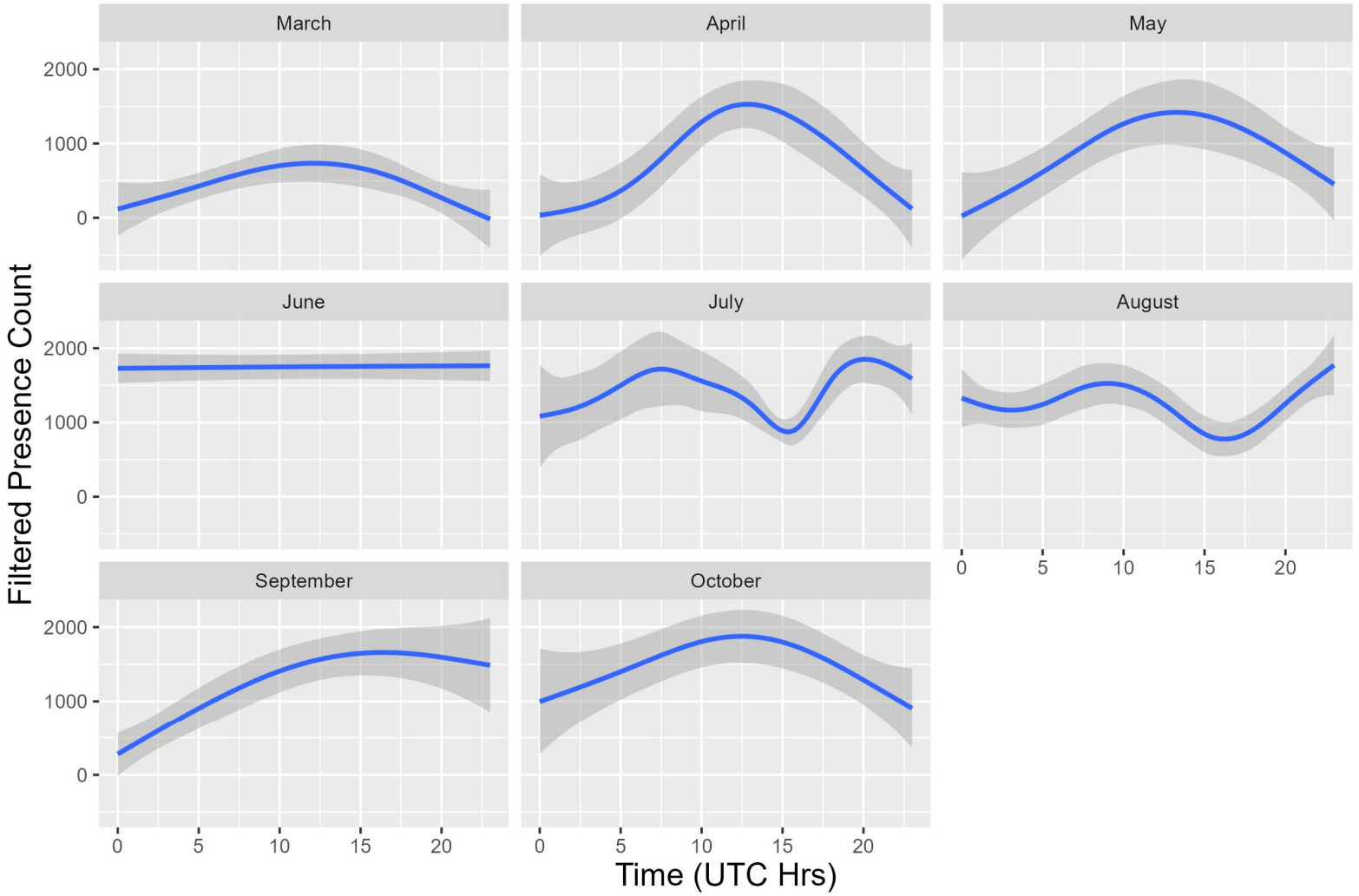

Figure 3. Hourly mean counts of filtered insect presence (blue) over the diurnal and seasonal cycles. The grey area represents the 95% confidence interval built from daily data. Time is given in hours from midnight (00:00), in UTC. These lines were derived using the LOESS curve function in the ggplot2 package (version 3.4.4; Wickham, 2016 [86]) for R 4.2.2; R Core Team, 2022 [87].

In our analysis of the outcomes of niche modelling, which compared response of insect aerial activity to high-altitude ('Aerial') versus surface ('Terrestrial') level conditions, we identified that the strongest source of variability in model predictive skill (in terms of the ROC and TSS statistics) was the level of subsampling performed prior to modelling (ANOVA, $F_{2,2693} = 223.67$, $p < 0.001$; Tukey HSD, 0.01 vs. 0.001, diff = 0.117, $p < 0.001$; 0.01 vs. 0.005, diff = −0.068, $p < 0.001$; 0.001 vs. 0.005, diff = 0.185, $p < 0.001$). The model algorithm also produced a relatively strong impact on predictions (ANOVA, $F_{2,2693} = 154.05$, $p < 0.001$; Tukey HSD, RF vs. CTA, diff = 0.138, $p < 0.001$; RF vs. GLM, diff = 0.131, $p < 0.001$; CTA vs. GLM, diff = 0.008, $p = 0.629$) compared with our choice of variables, which overall produced a weak impact on the average model accuracies (ANOVA, $F_{2,2693} = 55.91$, $p < 0.001$; Tukey HSD, Aerial vs. Terrestrial, diff = 0.05, $p < 0.001$; Aerial vs. Aerial + Terrestrial, diff = 0.09, $p < 0.001$; Terrestrial vs. Aerial + Terrestrial, diff = −0.043, $p < 0.001$). Next, we tried to predict insect aerial presence with niche models based on atmospheric variables sampled from high-altitude (aerial) versus surface conditions (terrestrial). Comparing findings from the aerial and terrestrial models, we found that niche models using only terrestrial variables (Table 1) outperformed those built with aerial variables during model evaluation (Table 1) (one-tailed Welch's *t*-test, T = −5.43, $p < 0.001$). However, a model combining both aerial and terrestrial conditions outperformed models containing only aerial or terrestrial variables in both instances (one-tailed Welch's *t*-test, Aerial + Terrestrial vs. Aerial, T = 9.57, $p < 0.001$; Aerial + Terrestrial vs. Terrestrial, T = 9.14, $p < 0.001$). The average predictive skill for niche models, including aerial variables, was 0.785 for ROC and 0.557 for TSS statistics, while the average predictive skill for models built only using terrestrial variables was 0.819 ROC and 0.607 TSS (Table A4). Although both surface-level conditions and aerial conditions contain good predictors of aerial insect activity, when taken independently (Figure 4, ROC >> 0.5, TSS >> 0), the models with the best predictive skill in our analysis combined variables from both the surface and the aerial environments (Table A4, Figure 4). The average predictive skill for these combined models was 0.837 for ROC and 0.651 for TSS statistics. We also observed an average gain of 0.018 ROC and 0.043 TSS, whenever aerial variables were included in addition to terrestrial, in the ENM.

Of our chosen model algorithms, GLMs performed only marginally better than CTAs (Tukey HSD, GLM versus CTA, diff = 0.008, $p = 0.629$), whereas RFs were significantly more accurate models than GLMs and CTAs on average (Tukey HSD, RF versus GLM, diff = 0.131, $p < 0.001$; RF versus CTA, diff = 0.139, $p < 0.001$; Table A4; Figure 4). There were no substantial differences in predictive skill between decision tree models and linear regression in this analysis (Table A4; Figure 4). Thus, we do not observe significant effects from algorithm complexity or type on model predictive skill for aeroecological data, meaning we cannot offer a conclusive recommendation on which algorithm to favour in future work. Algorithms will need to continue to be decided on a case-by-case basis [88,89].

We note that the above statistical tests of niche model evaluation metrics (ROC and TSS) were limited to TSS, as TSS and ROC evaluations proved to be highly correlated (Spearman's $\rho > 0.90$ and $p < 0.001$ in all cases). TSS values were further confirmed to be nonnormal through a Kolmogorov–Smirnov test against the normal distribution (D = 0.52, $p < 0.001$).

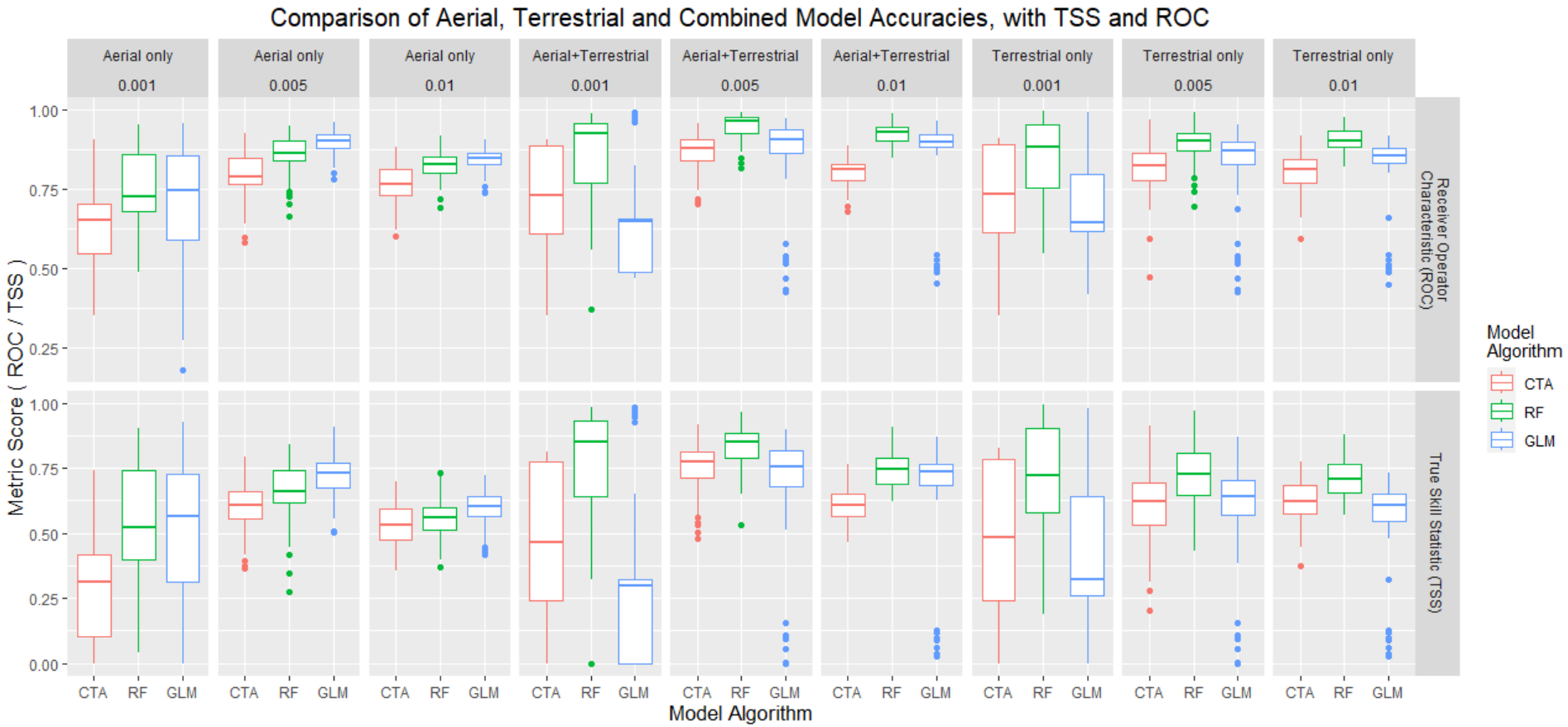

Figure 4. Boxplot comparison of models built with aerial variables (on pressure levels), terrestrial variables (surface only), and models combining the two. The plot is gridded into panels of model type (top), combining the variables used (upper text) and the subsampling factor (lower text). Each box-and-whisker represents the validation outcomes of 100 runs. Note the difference in scale between the Receiver Operator Curve (ROC, range 0–1) and True Skill Statistic (TSS, range −1—1). CTA—Classification Tree Analysis, GLM—Generalised Linear Model, RF—Random Forest.

We identified four primary atmospheric correlates of aerial insect activity using averages of biomod2's variable importance metric across the proportion of arable land cover (~0.47, Table A5), the ±500 m altitude band (~0.26, Table A5), surface and air temperatures (2 m, ~0.20; at height, ~0.16; Table A5), and the relative humidity (~0.15, Table A5). Notable variables in the middle ranks of variable importance (~0.03–0.04, Table A5) included the zonal windspeed and coniferous wood proportion (Table A5).

We found significant variability in biomod2's variable importance metric, depending on the model algorithm used (ANOVA, $p < 0.001$ for all contributing factors, Table A3). While the rank order of the variable importances was clear (Table A5), this indicated a degree of uncertainty in the magnitude of relative contributions. Hence, caution was applied when making inferences about the specific magnitude of the effect of different variables. The primary source of variability in calculated importance was found to be the selection of environmental variables in aerial and terrestrial models (Table A3). However, in models combining aerial and terrestrial variables, the choice of algorithm proved to be a more substantial contributor to variable importances than to model evaluation metrics and became the primary source of variability (Figure 5, Table A3). The subsampling factor was also a significant but comparatively weak contributor to variable importance (Figure 5, Table A3; $p < 0.001$).

The response curves of the ENMs allowed us to explore critical environmental thresholds for flight, as estimated probability of presence varied (Figure 6). However, we were unable to identify unambiguous critical thresholds for flight, as estimated probability of presence varied substantially by the ENM algorithm. This was caused by the underlying modelling approaches in each algorithm and were beyond the scope of this study to explore. However, we were able to determine some approximate thresholds by noting the broad patterns in response curve shape across algorithms (Figure 6, coloured lines per panel). The model response curves predicted an increased probability of presence within lower altitude bands (0–500 m, 500–1500 m), although activity at higher bands was expected to remain above 0.25 probability of presence, on average (Figure 6). By comparing the elevated probability of presence associated with increased surface and aerial temperatures (>20 °C, Figure 6) in ECMWF UK forecasts, we posited that common patterns of habitat suitability could be linked to seasonal and diurnal temperature trends across the UK, with limited regulation from national-scale bands of rain and moisture (Figure 7. We further noted that elevated probability of presence in voxels associated with increased arable land proportion (>60% Figure 6) appeared to be responsible for localising ('clumping') patches of high probability of presence in the projection map (Figure 7). However, as the Chilbolton study site consists of mostly arable land, this model may not hold true for all UK insect populations. The models on which the response curves were based can also be used to visualise how the spatial distribution of environmental variables may alter the suitability of a habitat, as shown through our niche model projections of the whole of the UK (Figure 7). However, we emphasise that this analysis is speculative, as the niche models can only identify areas similar to those where we have observed flight on the WSR and are not a substitute for physiological and behavioural studies.

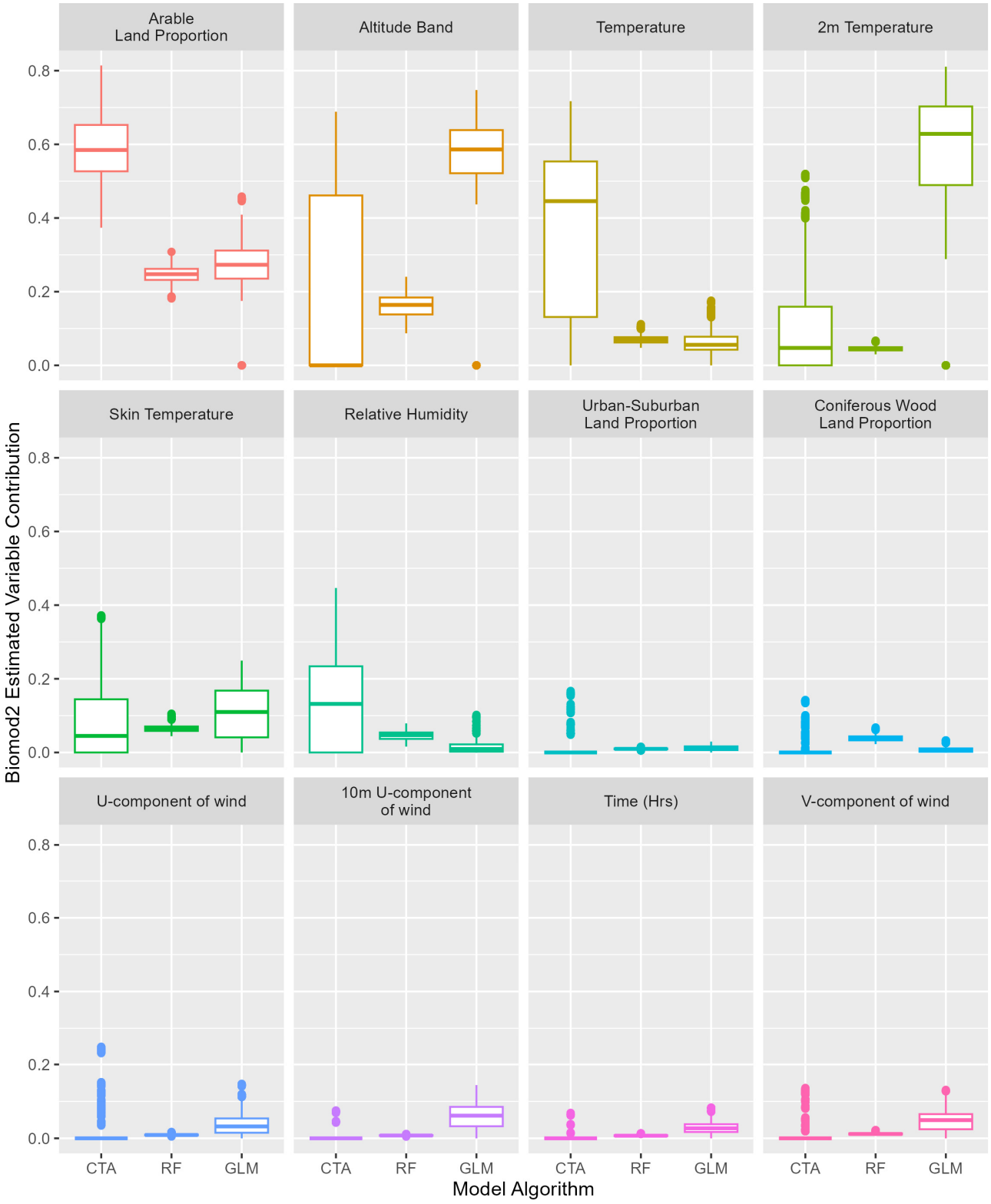

Figure 5. Biomod2 estimated variable importances for all variables used in this study, apart from vertical velocity, U-component of wind (zonal wind), potential vorticity, and divergence (which have an average contribution of <0.15 for all models). Variables are sorted by averaged rank order of importance and taken from the aerial–terrestrial combined model with a subsampling factor of 0.1%. Variable importance (*y*-axis) is measured in 1—Pearson's correlation coefficient (0–1); see Section 2.2.4 for further details. Note the variability by model algorithm. CTA—Classification Tree Analysis, GLM—Generalised Linear Model, RF—Random Forest.

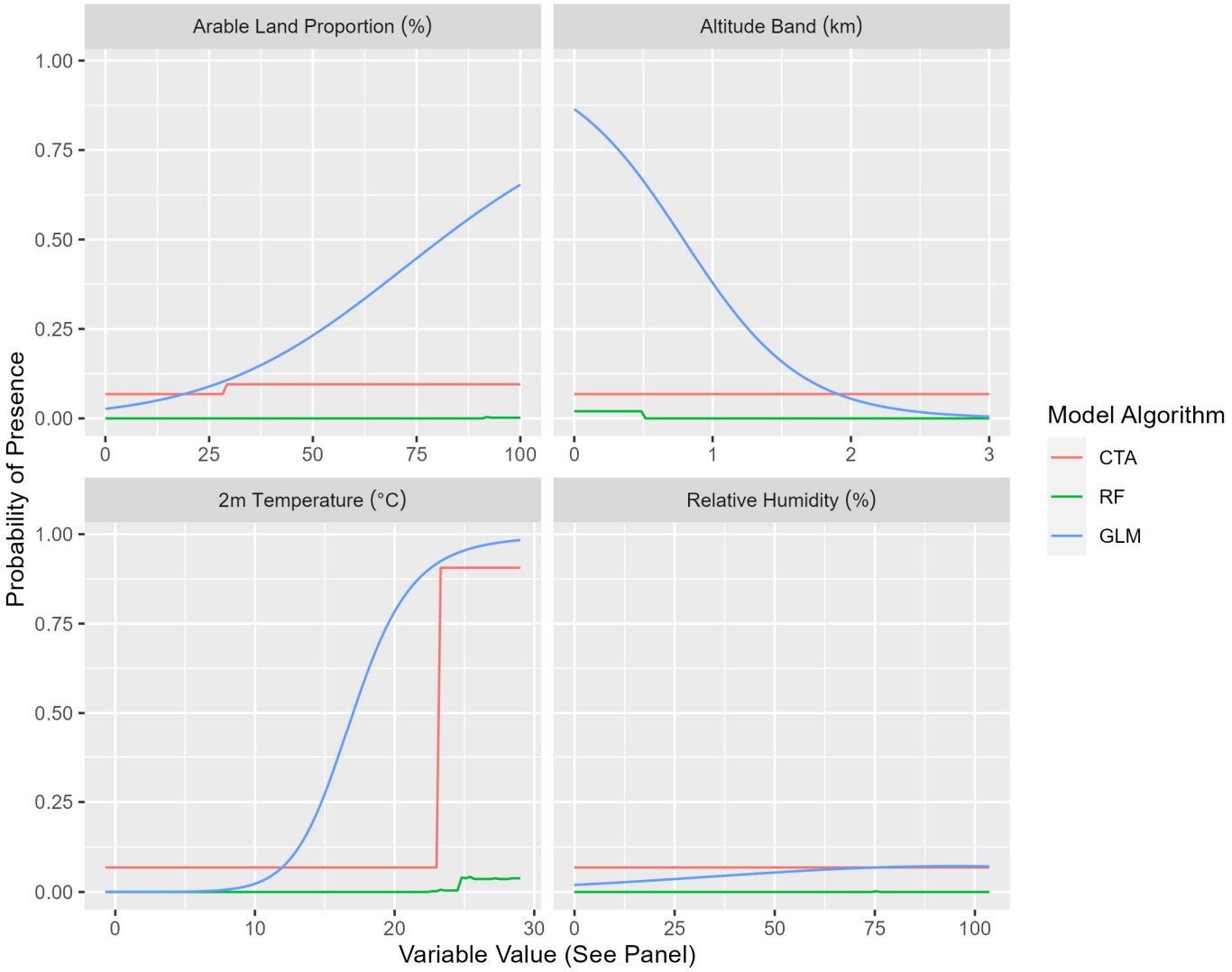

Figure 6. Response curves for the top four contributing variables; curves are taken from 'combined' models with both aerial and terrestrial variables, for subsampling factor 0.01. The response curves are based on the model run with the best predictive skill (in terms of ROC and TSS) out of each set of 100. 'Altitude band' is given as a categorical variable where the number in km represents the median of the band (i.e., 1 km ± 0.5 km). CTA—Classification Tree Analysis, GLM—Generalised Linear Model, RF—Random Forest.

In summary, our analysis showed that aerial variables are strong predictors of activity when used independently of terrestrial predictors, but terrestrial predictors are the stronger of the two, and the models with the best predictive skill combined both. Our analysis of the three treatment groups (Aerial, Terrestrial, Aerial + Terrestrial) demonstrated that niche models with atmospheric variables are well suited to modelling insect aerial activity, and models combining both terrestrial and aerial conditions performed significantly better than any model using terrestrial or aerial only. We have highlighted the primary abiotic covariates of insect flight for the Chilbolton community in 2017, using our comparison of variable importances: where insect activity was positively associated with increasing arable land proportion, temperature at-height and at-surface, and relative humidity. We also noted strong seasonal patterns in the diurnal cycle of insect flight activity, and a speculative connection between environmental stimuli of insect flight and national-level weather patterns.

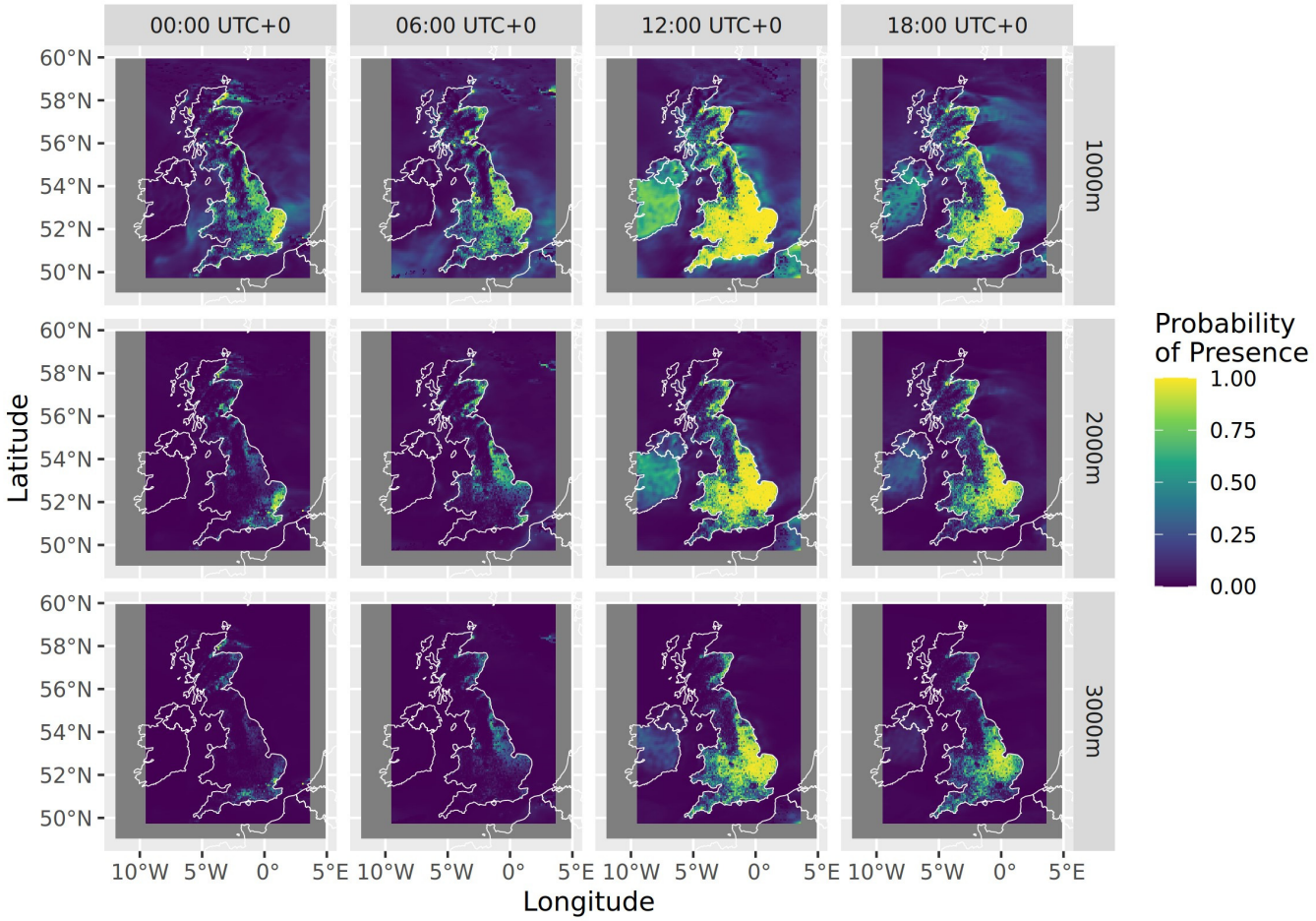

Figure 7. Predictions of aerial habitat suitability (probability of presence) from the median predictive skill (in terms of TSS) GLM of insect activity (0.01 subsampling factor, aerial and terrestrial variables). Predictions were made using atmospheric data from 17 July 2017 at 00:00, 06:00, 12:00, and 18:00 h UTC (columns). Atmospheric data were taken from three altitude levels, 1000 m, 2000 m, and 3000 m above sea level (rows). This shows where similar atmospheric environments associated with insects occurred across the UK on this day, and how the suitable area developed over time.

4. Discussion

In this study, we describe a new method for extending environmental niche modelling to high-altitude biological observations, which has been strongly argued for by the aeroecological community [39,62]. Such an approach theoretically allows researchers to describe insect active dispersal, the consequences of dispersal for meta-populations, and conservation under climate change [90–93]. We demonstrate that niche models incorporating atmospheric variables outperform those using information from the surface level only. We also note that insect occurrence in the aerosphere is most closely associated with arable land and temperature at the surface below, as well as temperature and relative humidity at-height.

TSS and ROC values from terrestrial niche models were significantly increased when the model included aerial variables (on average, +0.018 ROC and +0.043 TSS). Therefore, the model accuracy and variable importance metrics show that insect presence at high altitude may be better explained by including atmospheric conditions above the surface level, but ENMs achieve their highest predictive power when combining predictor variables from both the surface and the aerial environment (Figure 4). The outcome was that our primary hypothesis is inconclusive. We expect this finding was due to conflating

factors such as the inability to distinguish between atmospheric influence on take-off and flight adjustment behaviours, which theoretically were more affected by conditions at surface and in the air column, respectively. To show definitively that high-altitude (aerial) variables are more accurate predictors of insect aerial activity compared with surface (terrestrial) variables, analysis of a wider range of radar sites will be required. Model variability resulting from model algorithm will also require further consultation with the ecological modelling community, to understand the uncertainties in each approach [88,89].

Our niche model analysis has indicated that atmospheric humidity perhaps plays a more dominant role in enabling insect flight than has been suggested by the current literature [21,70,72]. By contrast, windspeed and ground temperature are well documented as limiting factors in insect flight activity [45,70,72,94,95]. However, there is inconsistency in and disagreement on the importance of relative humidity, as well as the mechanism by which it affects insect flight: several papers claim that flight behaviour is affected by changes in relative humidity [96,97], that humidity is a secondary regulator and modulates behavioural responses to temperature [21,72], and that humidity plays no significant role in flight behaviour at all [70,98]. The entomological literature further suffers from a lack of comparable results due to the wide range of study species, locations, and experimental designs (e.g., controlled conditions, ground-level field experiment, tracking of individual flight) [72,94,96,98]. As a species' dispersal strategy determines flight behaviour, geographical differences in the structure of insect communities could also influence the importance of predictor variables. Further investigation of the physiological and behavioural mechanisms of flight will be needed to validate future niche models, as well as prospective insect forecast tools.

Our niche model analysis further indicated a highly positive relationship between arable land cover and the probability of presence. By contrast, the previous literature has described a negative association between arthropod diversity and intensively farmed land, with a similar relationship reported for abundance [99–101]. However, studies have shown that the consequences for arable land on insects can depend on the land management practises, e.g., the use of chemicals and fertiliser, or grazing by sheep and cattle [99,102]. Our findings can be explained by the dominant habitats in the vicinity of the radar, which comprise arable land with patches of broadleaf wood, with coniferous woodland, grassland, and urban–suburban land found in relatively small proportions (<20% cover). The prevalence of insect activity over arable land is possibly caused by the intermingling of natural communities and pest species associated with crops. However, the CEH arable land classification, according to Jackson (2000) [103], comprises a range of cropland types, including intensively farmed land alongside annual leys and fallow land. Therefore, we are not able to distinguish the effect of different land management practises in this study. Further, as the Chilbolton site offers limited spatial heterogeneity, and the CEH land cover is far more granular than our radar observations, our niche models are unable to meaningfully analyse the effect of habitat gradients on high-flying insect abundance (see Henrys and Jarvis (2019) [104] for further discussion of the importance of spatial resolution when integrating ground survey and remote sensing data). However, by adopting the methodology we demonstrate here with a national-scale weather surveillance radar network, it would be possible to sample a broader range of habitat types and gradients.

Whether working at the local or national scale, an ongoing challenge of studying insects with radars is the filtering procedure. A shortcoming of our observations of insect activity is that several of the filtering stages are based on fixed thresholds, such as the non-meteorological and meteorological filter from Kilambi et al. (2018) [80]. Fixed thresholds ignore potential overlap between radar signatures attributed to different scatterers, especially for birds and insects [105–107], leading to false presences and potentially to false correlations in later niche modelling. Certain meteorological phenomena can also be responsible for false presences (e.g., melting layers; see Baldini and Gorgucci, 2006; Ryzhkov and Krause, 2022 [108,109]), which we noted on certain days of NXPol-1 observations,

where large rainclouds were present over the radar site. Single events such as sun spikes, interference from other radio sources, and chaff from military exercises can contribute to erroneous presences identified in filtering, which continues to necessitate manual data cleaning before further analysis. Radar instrumentation is also inherently range-biased by the sensitivity of the system, as the power density of the beam decreases over distance, and the return signal suffers attenuation in the atmosphere (see Rocchini et al., 2023 [110] for a discussion of the impact of spatial bias in ecological modelling). This and the need to carry out manual data cleaning (where confirmation bias can be introduced) with no supporting at-height validation data introduces uncertainty into any spatial analysis performed downstream. This points to an urgent need for further, closer collaboration between the radar science and ecology communities to ensure radar observations are properly validated and understood in the ecological context that future aeroecology work can meet the best practises of both fields. WSR observations of presence could benefit in future from improvements to classification accuracy and error quantification, either through machine learning algorithms of existing radar data, to better distinguish target classes [82,105,111], or ideally through cooperative field campaigns led jointly between atmospheric scientists and ecologists. As noted previously, there is also a lack of species specificity in WSR biological observations, including those produced by our filtering of NXPol-1. Recent work with VLRs has shown promise of remedying this problem, as they are capable of identifying individual insect morphotypes from their ventral reflectivity signatures, as well as accurately determining their headings as they pass through the radar beam [16,56,112,113]. Thus, a potential solution to the limitations of both WSR and VLR systems could be to carry out joint radar experiments with WSR and VLR, backed up with field ground truthing.

Our results illustrated an association between insect presence–absence over time and conditions tied to local weather and ground habitat (arable land cover, temperature, and humidity). Previous work has further indicated that national-level weather patterns play an indirect role in insect flight and reproductive behaviour by regulating local temperature, humidity, and groundwater [114–117]. These variables are particularly shaped by the distribution of frontal zones between cold and warm air masses, which implies that insect reproduction and mass emergences could be responsive to these weather patterns. If true, this relationship would render local insect activity more predictable and would require little alteration to existing weather forecasting infrastructure. Further tools that adapt existing niche-model approaches from the terrestrial and marine environments will allow future aeroecological studies to quickly build and describe probabilistic relationships between many collinear variables and the probability of presence of aerial organisms, without the need for regular, wide-ranging, and costly field campaigns. However, it remains prudent to continue to carry out localised field investigations of insect flight and behaviour in the aerosphere to continue to ground-truth observations from radars. Controlled experiments will also be essential to understand the mechanistic causes of in-flight habitat selection in insects, which cannot be definitively described with remote sensing alone (see [72,98]).

Supplementary Materials: The following supporting information can be downloaded at: https://www.mdpi.com/article/10.3390/rs16234388/s1, Video S1: RawAndKilambi2017.mp4.

Author Contributions: Conceptualization, S.H., R.N.III, and C.H.; methodology, S.H.; software, S.H. and R.N.III; validation, S.H.; formal analysis, S.H.; investigation, S.H.; resources, R.N.III and C.H.; data curation, R.N.III; writing—original draft preparation, S.H.; writing—review and editing, S.H., R.N.III, and C.H; visualisation, S.H.; supervision, R.N.III and C.H.; project administration, R.N.III; funding acquisition, R.N.III. All authors have read and agreed to the published version of the manuscript.

Funding: This research was supported by a PANORAMA PhD studentship to SH from the Natural Environment Research Council, grant number NE/S007458/1. The APC was funded by the University of Leeds.

Data Availability Statement: The WSR data for this study are available freely from CEDA. See Bennett (2020) [118] for more information. All ECMWF data can be acquired freely from the ECMWF operational archive, via the MARS catalogue (https://www.ecmwf.int/en/forecasts/dataset/operational-archive, accessed 26 November 2023). Presence–absence–environment tables used in biomod2 analysis can be found in the following GitHub repository (https://github.com/SamuelHodges/Weather-Radars-Reveal-Environmental-Conditions-for-High-Altitude-Insect-Movement-Through-the-Aerosp, accessed 7 November 2024).

Acknowledgments: We would like to acknowledge Laurents Marker for supporting our early efforts to engage downscaling atmospheric models, Lindsay Bennett and David Dufton for their assistance and tutorship in interpreting WSR metrics and PPIs, as well as Weronika Osmolska and Andrew Martin for helping review this manuscript. The authors would like to acknowledge the Atmospheric Measurement and Observation Facility (AMOF) a Natural Environment Research Council (UKRI-NERC) funded facility (NE/Y005376/1), for providing the processed NXPol-1 radar data used in our analysis.

Conflicts of Interest: The authors declare no conflicts of interest.

Appendix A

Table A1. Auto-correlation matrix of Spearman's ρ for all variables used in this study, based on the presence–absence table for 2017 with subsampling factor 0.01. Values with high correlation are highlighted in yellow/green ($\rho > 0.6$, $0.6 > \rho > 0.3$) and values with little correlation are highlighted in blue ($\rho < 0.3$). Auto-correlation is chiefly present in similar variables measured from different heights (wind and temperature), but also includes a correlation between the relative humidity ('r') and large-scale rain rate ('lsrr').

	Altitude	Temperature	Relative Humidity	Zonal Windspeed	Meridional Windspeed	Atmospheric Divergence	Potential Vorticity	Relative Vorticity	Vertical Velocity	10 m Wind Gust	10 m Zonal Windspeed
Altitude	1.000	−0.640	−0.440	0.210	−0.072	−0.023	0.073	0.010	0.009	0.017	0.018
Temperature	−0.640	1.000	0.280	0.150	0.330	−0.019	−0.096	−0.064	−0.099	0.007	0.130
Relative Humidity	−0.440	0.280	1.000	0.013	0.080	0.046	−0.240	−0.061	−0.033	0.059	0.099
Zonal Windspeed	0.210	0.150	0.013	1.000	0.078	−0.043	0.049	0.031	−0.056	0.120	0.680
Meridional Windspeed	−0.072	0.330	0.080	0.078	1.000	−0.011	−0.120	−0.065	−0.130	−0.019	−0.220
Atmospheric Divergence	−0.023	−0.019	0.046	−0.043	−0.011	1.000	−0.048	−0.047	−0.018	−0.025	−0.040
Potential Vorticity	0.073	−0.096	−0.240	0.049	−0.120	−0.048	1.000	0.660	0.020	0.071	0.058
Relative Vorticity	0.010	−0.064	−0.061	0.031	−0.065	−0.047	0.660	1.000	−0.028	0.077	0.048
Vertical Velocity	0.009	−0.099	−0.033	−0.056	−0.130	−0.018	0.020	−0.028	1.000	−0.006	0.002
10 m Wind Gust	0.017	0.007	0.059	0.120	−0.019	−0.025	0.071	0.077	−0.006	1.000	0.140
10 m Zonal Windspeed	0.018	0.130	0.099	0.680	−0.220	−0.040	0.058	0.048	0.002	0.140	1.000
10m Meridional Windspeed	0.001	0.250	0.047	0.390	0.490	−0.024	−0.068	−0.110	−0.055	−0.130	0.200
2 Temperature	0.009	0.520	0.220	0.350	0.250	−0.018	−0.036	0.053	−0.092	0.160	0.280
Convective Rain Rate	0.004	−0.001	0.120	0.089	−0.015	−0.002	0.019	0.049	−0.058	0.130	0.120
Large Scale Rain Rate	0.028	0.011	0.200	0.170	−0.024	−0.010	0.032	0.037	−0.046	0.210	0.170
Skin Temperature	0.013	0.440	0.190	0.290	0.190	−0.013	−0.020	0.059	−0.080	0.210	0.250
Broadleaf Wood Proportion	−0.100	0.043	0.064	0.002	0.004	−0.012	−0.016	−0.009	0.021	−0.100	−0.016
Urban Suburban Proportion	−0.051	0.005	0.039	0.029	0.004	0.001	−0.001	0.011	−0.010	−0.120	−0.009

Coniferous Wood Proportion	−0.095	0.061	0.049	−0.024	0.002	−0.010	−0.010	0.007	0.009	−0.038	−0.013
Arable Land Proportion	−0.081	0.008	0.053	0.010	−0.002	−0.011	0.001	−0.008	0.027	−0.110	0.000
Grassland Proportion	−0.024	0.016	0.010	−0.004	0.007	−0.009	−0.004	0.004	0.005	−0.019	−0.007

	10 m Meridional Windspeed	2 m Temperature	Convective Rain Rate	Large Scale Rain Rate	Skin Temperature	Broadleaf Wood Proportion	Urban Suburban Proportion	Coniferous Wood Proportion	Arable Land Proportion	Grassland Proportion
Altitude	0.001	0.009	0.004	0.028	0.013	−0.100	−0.051	−0.095	−0.081	−0.024
Temperature	0.250	0.520	−0.001	0.011	0.440	0.043	0.005	0.061	0.008	0.016
Relative Humidity	0.047	0.220	0.120	0.200	0.190	0.064	0.039	0.049	0.053	0.010
Zonal Windspeed	0.390	0.350	0.089	0.170	0.290	0.002	0.029	−0.024	0.010	−0.004
Meridional Windspeed	0.490	0.250	−0.015	−0.024	0.190	0.004	0.004	0.002	−0.002	0.007
Atmospheric Divergence	−0.024	−0.018	−0.002	−0.010	−0.013	−0.012	0.001	−0.010	−0.011	−0.009
Potential Vorticity	−0.068	−0.036	0.019	0.032	−0.020	−0.016	−0.001	−0.010	0.001	−0.004
Relative Vorticity	−0.110	0.053	0.049	0.037	0.059	−0.009	0.011	0.007	−0.008	0.004
Vertical Velocity	−0.055	−0.092	−0.058	−0.046	−0.080	0.021	−0.010	0.009	0.027	0.005
10m Wind Gust	−0.130	0.160	0.130	0.210	0.210	−0.100	−0.120	−0.038	−0.110	−0.019
10m Zonal Windspeed	0.200	0.280	0.120	0.170	0.250	−0.016	−0.009	−0.013	0.000	−0.007
10m Meridional Windspeed	1.000	0.220	−0.012	0.059	0.140	0.058	0.077	−0.002	0.072	0.013
2m Temperature	0.220	1.000	0.170	0.110	0.960	−0.130	−0.100	−0.060	−0.140	−0.044
Convective Rain Rate	−0.012	0.170	1.000	0.290	0.190	−0.023	−0.018	−0.015	−0.025	−0.013
Large Scale Rain Rate	0.059	0.110	0.290	1.000	0.110	−0.068	−0.053	−0.038	−0.069	−0.010
Skin Temperature	0.140	0.960	0.190	0.110	1.000	−0.170	−0.140	−0.081	−0.180	−0.054
Broadleaf Wood Proportion	0.058	−0.130	−0.023	−0.068	−0.170	1.000	0.440	0.480	0.340	0.073
Urban Suburban Proportion	0.077	−0.100	−0.018	−0.053	−0.140	0.440	1.000	0.120	0.230	0.039
Coniferous Wood Proportion	−0.002	−0.060	−0.015	−0.038	−0.081	0.480	0.120	1.000	0.090	0.090

Arable Land Proportion	0.072	−0.140	−0.025	−0.069	−0.180	0.340	0.230	0.090	1.000	0.095
Grassland Proportion	0.013	−0.044	−0.013	−0.010	−0.054	0.073	0.039	0.090	0.095	1.000

Table A2. Auto-correlation matrix of Spearman's ρ p-values for all variables used in this study, based on the presence–absence table for 2017 with subsampling factor 0.01. Significant values are highlighted in yellow ($p < 0.05$), partially significant values in green ($p < 0.1$), and non-significant values in blue ($p > 0.1$). Cells shaded in black contain values where p was too small to properly represent in R (p~0.00). The majority of the correlation tests proved to be significant, however, these should be interpreted alongside the associated ρ value to check whether the correlation is likely to be impactful.

	Altitude	**Temperature**	**Relative Humidity**	**Zonal Windspeed**	**Meridional Windspeed**	**Atmospheric Divergence**	**Potential Vorticity**	**Relative Vorticity**	**Vertical Velocity**	**10m Wind Gust**	**10m Zonal Windspeed**
Altitude	0.000	0.000	0.000	0.000	0.000	0.000	0.000	0.060	0.090	0.000	0.000
Temperature	0.000	0.000	0.000	0.000	0.000	0.000	0.000	0.000	0.000	0.180	0.000
Relative Humidity	0.000	0.000	0.000	0.010	0.000	0.000	0.000	0.000	0.000	0.000	0.000
Zonal Windspeed	0.000	0.000	0.010	0.000	0.000	0.000	0.000	0.000	0.000	0.000	0.000
Meridional Windspeed	0.000	0.000	0.000	0.000	0.000	0.050	0.000	0.000	0.000	0.000	0.000
Atmospheric Divergence	0.000	0.000	0.000	0.000	0.050	0.000	0.000	0.000	0.000	0.000	0.000
Potential Vorticity	0.000	0.000	0.000	0.000	0.000	0.000	0.000	0.000	0.000	0.000	0.000
Relative Vorticity	0.060	0.000	0.000	0.000	0.000	0.000	0.000	0.000	0.000	0.000	0.000
Vertical Velocity	0.090	0.000	0.000	0.000	0.000	0.000	0.000	0.000	0.000	0.300	0.720
10m Wind Gust	0.000	0.180	0.000	0.000	0.000	0.000	0.000	0.000	0.300	0.000	0.000
10m Zonal Windspeed	0.000	0.000	0.000	0.000	0.000	0.000	0.000	0.000	0.720	0.000	0.000
10m Meridional Windspeed	0.810	0.000	0.000	0.000	0.000	0.000	0.000	0.000	0.000	0.000	0.000
2 Temperature	0.090	0.000	0.000	0.000	0.000	0.000	0.000	0.000	0.000	0.000	0.000
Convective Rain Rate	0.450	0.830	0.000	0.000	0.010	0.710	0.000	0.000	0.000	0.000	0.000
Large-Scale Rain Rate	0.000	0.040	0.000	0.000	0.000	0.070	0.000	0.000	0.000	0.000	0.000
Skin Temperature	0.020	0.000	0.000	0.000	0.000	0.020	0.000	0.000	0.000	0.000	0.000
Broadleaf Wood Proportion	0.000	0.000	0.000	0.660	0.470	0.030	0.000	0.090	0.000	0.000	0.000

Urban Suburban Proportion	0.000	0.400	0.000	0.000	0.460	0.910	0.860	0.050	0.060	0.000	0.110
Coniferous Wood Proportion	0.000	0.000	0.000	0.000	0.750	0.080	0.060	0.180	0.120	0.000	0.010
Arable Land Proportion	0.000	0.130	0.000	0.070	0.770	0.040	0.870	0.170	0.000	0.000	0.990
Grassland Proportion	0.000	0.000	0.070	0.450	0.240	0.110	0.500	0.450	0.340	0.000	0.220

	10m Meridional Windspeed	2m Temperature	Convective Rain Rate	Large-Scale Rain Rate	Skin Temperature	Broadleaf Wood Proportion	Urban Suburban Proportion	Coniferous Wood Proportion	Arable Land Proportion	Grassland Proportion
Altitude	0.810	0.090	0.450	0.000	0.020	0.000	0.000	0.000	0.000	0.000
Temperature	0.000	0.000	0.830	0.040	0.000	0.000	0.400	0.000	0.130	0.000
Relative Humidity	0.000	0.000	0.000	0.000	0.000	0.000	0.000	0.000	0.000	0.070
Zonal Windspeed	0.000	0.000	0.000	0.000	0.000	0.660	0.000	0.000	0.070	0.450
Meridional Windspeed	0.000	0.000	0.010	0.000	0.000	0.470	0.460	0.750	0.770	0.240
Atmospheric Divergence	0.000	0.000	0.710	0.070	0.020	0.030	0.910	0.080	0.040	0.110
Potential Vorticity	0.000	0.000	0.000	0.000	0.000	0.000	0.860	0.060	0.870	0.500
Relative Vorticity	0.000	0.000	0.000	0.000	0.000	0.090	0.050	0.180	0.170	0.450
Vertical Velocity	0.000	0.000	0.000	0.000	0.000	0.000	0.060	0.120	0.000	0.340
10m Wind Gust	0.000	0.000	0.000	0.000	0.000	0.000	0.000	0.000	0.000	0.000
10m Zonal Windspeed	0.000	0.000	0.000	0.000	0.000	0.000	0.110	0.010	0.990	0.220
10m Meridional Windspeed	0.000	0.000	0.030	0.000	0.000	0.000	0.000	0.710	0.000	0.020
2m Temperature	0.000	0.000	0.000	0.000	0.000	0.000	0.000	0.000	0.000	0.000

Convective Rain Rate	0.030	0.000	0.000	0.000	0.000	0.000	0.000	0.010	0.000	0.010
Large-Scale Rain Rate	0.000	0.000	0.000	0.000	0.000	0.000	0.000	0.000	0.000	0.070
Skin Temperature	0.000	0.000	0.000	0.000	0.000	0.000	0.000	0.000	0.000	0.000
Broadleaf Wood Proportion	0.000	0.000	0.000	0.000	0.000	0.000	0.000	0.000	0.000	0.000
Urban Suburban Proportion	0.000	0.000	0.000	0.000	0.000	0.000	0.000	0.000	0.000	0.000
Coniferous Wood Proportion	0.710	0.000	0.010	0.000	0.000	0.000	0.000	0.000	0.000	0.000
Arable Land Proportion	0.000	0.000	0.000	0.000	0.000	0.000	0.000	0.000	0.000	0.000
Grassland Proportion	0.020	0.000	0.010	0.070	0.000	0.000	0.000	0.000	0.000	0.000

Table A3. Summary table of F and *p* values from analysis of variance tests carried out on biomod2's estimates of variable importances, per model type (combined/aerial/terrestrial). In all estimates of variable importance for all models, the environment variable used provided the greatest source of variation.

ANOVA Statistic	F-Value			*p*-Value		
Model Type	**Combined**	**Aerial**	**Terrestrial**	**Combined**	**Aerial**	**Terrestrial**
Variable Name	10604.9	2295.61	5993.0	$<2e^{-16}$	$<2e^{-16}$	$<2e^{-16}$
Subsampling Factor	311.9	78.86	268.2	$<2e^{-16}$	$<2e^{-16}$	$<2e^{-16}$
Algorithm	15168.6	382.29	3604.5	$<2e^{-16}$	$<2e^{-16}$	$<2e^{-16}$

Table A4. Mean niche model accuracy scores from validation. Scores included are the area under the curve (AUC) value from Receiver Operator Curves (ROCs) and the True Skill Statistic (TSS). This study compares the impact of the model algorithm (rows), variables used, and subsampling factor (columns). Scores are coloured from red (0.5/0) to yellow (0.65/0.3) to green (0.9/1) according to the skill of the model (worst to poor to best). See also Figure 6. CTA—Classification Tree Analysis, GLM—Generalised Linear Model, RF—Random Forest.

	Environment Variable Types	**Aerial**			**Aerial + Terrestrial**			**Terrestrial**		
Model Algorithm	**Subsampling Fraction / Evaluation Metric**	**0.001**	**0.005**	**0.01**	**0.001**	**0.005**	**0.01**	**0.001**	**0.005**	**0.01**
CTA	ROC	0.628	0.798	0.767	0.720	0.871	0.804	0.744	0.819	0.811
	TSS	0.277	0.602	0.531	0.467	0.760	0.612	0.518	0.612	0.627
GLM	ROC	0.701	0.900	0.845	0.642	0.871	0.863	0.699	0.836	0.820
	TSS	0.526	0.719	0.598	0.293	0.696	0.667	0.430	0.599	0.550
RF	ROC	0.739	0.861	0.825	0.884	0.950	0.927	0.839	0.897	0.907
	TSS	0.544	0.664	0.553	0.783	0.833	0.745	0.700	0.722	0.709

Table A5. List of mean variable importances by algorithm and variable. See Figure 5 for a visual representation of these values. The variable importances are presented here in rank order of the mean of all runs across algorithms (column 1). See Section 2.2.4 for a description of the biomod2 variable importance metric and supporting citations. CTA—Classification Tree Analysis, GLM—Generalised Linear Model, RF—Random Forest.

Explanatory Variable	**Mean Variable Importance**	**Mean CTA Variable Importance**	**Mean GLM Variable Importance**	**Mean RF Variable Importance**
Arable Land Proportion	0.468	0.697	0.445	0.262
Altitude Band (+500 m)	0.257	0.317	0.327	0.129
2m Temperature	0.195	0.131	0.379	0.073
Temperature	0.155	0.204	0.150	0.112
Relative Humidity	0.152	0.188	0.182	0.086
Skin Temperature	0.117	0.079	0.186	0.087
Zonal Wind	0.060	0.046	0.103	0.031
Coniferous Wood Proportion	0.046	0.042	0.034	0.062
10m Zonal Wind	0.046	0.008	0.116	0.014
Urban Suburban Land Proportion	0.045	0.027	0.089	0.019
Broadleaf Wood Proportion	0.042	0.020	0.086	0.020
Instantaneous 10 m Wind Gust	0.040	0.009	0.096	0.016
Large-Scale Rain Rate	0.038	0.022	0.079	0.015
Time (h)	0.037	0.027	0.060	0.024
Meridional Wind	0.033	0.018	0.049	0.032
10m Meridional Wind	0.032	0.008	0.065	0.021

Vertical Velocity	0.031	0.014	0.058	0.020
Grassland Proportion	0.029	0.007	0.071	0.010
Atmospheric Divergence	0.025	0.008	0.055	0.013
Potential Vorticity	0.021	0.009	0.018	0.035
Relative Vorticity	0.020	0.010	0.030	0.021
Convective Rain Rate	0.013	0.000	0.025	0.013

References

1. Crespo-Pérez, V.; Kazakou, E.; Roubik, D.W.; Cárdenas, R.E. The importance of insects on land and in water: A tropical view. *Curr. Opin. Insect Sci.* **2020**, *40*, 31–38. https://doi.org/10.1016/j.cois.2020.05.016.
2. Kenis, M.; Auger-Rozenberg, M.A.; Roques, A.; Timms, L.; Péré, C.; Cock, M.J.W.; Settele, J.; Augustin, S.; Lopez-Vaamonde, C. Ecological effects of invasive alien insects. *Biol. Invasions* **2009**, *11*, 21–45. https://doi.org/10.1007/s10530-008-9318-y
3. Verma, R.C.; Waseem, A.M.; Sharma, N.; Bharathi, K.; Singh, S.; Anto Rashwin, A.; Pandey, S.K.; Singh, B.V. The Role of Insects in Ecosystems, an in-depth Review of Entomological Research. *Int. J. Environ. Clim. Change* **2023**, *13*, 4340–4348.
4. Noriega, J.A.; Hortal, J.; Azcárate, F.M.; Berg, M.P.; Bonada, N.; Briones, M.J.I.; Del Toro, I.; Goulson, D.; Ibanez, S.; Landis, D.A.; et al. Research trends in ecosystem services provided by insects. *Basic Appl. Ecol.* **2018**, *26*, 8–23. https://doi.org/10.1016/j.baae.2017.09.006
5. Doak, D.F.; Morris, W.F. Demographic compensation and tipping points in climate-induced range shifts. *Nature* **2010**, *467*, 959–962. https://doi.org/10.1038/NATURE09439
6. Tomiolo, S.; Ward, D. Species migrations and range shifts: A synthesis of causes and consequences. *Perspect. Plant Ecol. Evol. Systematics* **2018**, *33*, 62–77. https://doi.org/10.1016/J.PPEES.2018.06.001
7. Cardoso, P.; Barton, P.S.; Birkhofer, K.; Chichorro, F.; Deacon, C.; Fartmann, T.; Fukushima, C.S.; Gaigher, R.; Habel, J.C.; Hallmann, C.A.; et al. Scientists' warning to humanity on insect extinctions. *Biol. Conserv.* **2022**, *242*, 108426. https://doi.org/10.1016/j.biocon.2020.108426
8. Chapman, J.W.; Reynolds, D.R.; Wilson, K. Long-range seasonal migration in insects: Mechanisms, evolutionary drivers and ecological consequences. *Ecol. Lett.* **2015**, *18*, 287–302. https://doi.org/10.1111/ele.12407
9. Boulanger, Y.; Fabry, F.; Kilambi, A.; Pureswaran, D.S.; Sturtevant, B.R.; Saint-Amant, R. The use of weather surveillance radar and high-resolution three dimensional weather data to monitor a spruce budworm mass exodus flight. *Agric. For. Meteorol.* 2017, 234–235, 127–135. https://doi.org/10.1016/j.agrformet.2016.12.018
10. Florio, J.; Verú, L.M.; Dao, A.; Yaro, A.S.; Diallo, M.; Sanogo, Z.L.; Samaké, D.; Huestis, D.L.; Yossi, O.; Talamas, E.; et al. Diversity, dynamics, direction, and magnitude of high-altitude migrating insects in the Sahel. *Sci. Rep.* **2020**, *10*, 20523. https://doi.org/10.1038/s41598-020-77196-7
11. Gandiaga, F.; James PM, A. Quantifying long-distance dispersal of an outbreaking insect species using trap capture data and phenology. *For. Ecol. Manag.* **2023**, *544*, 121187. https://doi.org/10.1016/j.foreco.2023.121187
12. Vavassori, L.; Saddler, A.; Müller, P. Active dispersal of Aedes albopictus: A mark-release-recapture study using self-marking units. *Parasites Vectors* **2019**, *12*, 583. https://doi.org/10.1186/s13071-019-3837-5
13. Cui, K.; Hu, C.; Wang, R.; Li, S.; Wu, D.; Ma, S. Quantifying insect migration across Bohai strait using weather radar. *J. Eng.* **2019**, *2019*, 6095–6098. https://doi.org/10.1049/joe.2019.0197.
14. Hawkes WL, S.; Walliker, E.; Gao, B.; Forster, O.; Lacey, K.; Doyle, T.; Massy, R.; Roberts, N.W.; Reynolds, D.R.; Özden, Ö.; Chapman, J.W.; et al. Huge spring migrations of insects from the Middle East to Europe: quantifying the migratory assemblage and ecosystem services. *Ecography* **2022**, *2022*, e06288. https://doi.org/10.1111/ecog.06288
15. Knoblauch, A.; Thoma, M.; Menz MH, M. Autumn southward migration of dragonflies along the Baltic coast and the influence of weather on flight behaviour. *Anim. Behav.* **2021**, *176*, 99–109. https://doi.org/10.1016/j.anbehav.2021.04.003
16. Chapman, J.W.; Reynolds, D.R.; Mouritsen, H.; Hill, J.K.; Riley, J.R.; Sivell, D.; Smith, A.D.; Woiwod, I.P. Wind Selection and Drift Compensation Optimize Migratory Pathways in a High-Flying Moth. *Curr. Biol.* **2008**, *18*, 514–518. https://doi.org/10.1016/j.cub.2008.02.080
17. Menz, M.H.M.; Scacco, M.; Bürki-Spycher, H.-M.; Williams, H.J.; Reynolds, D.R.; Chapman, J.W.; Wikelski, M. Individual Tracking Reveals Long-Distance Flight-Path Control in a Nocturnally Migrating Moth, 2022. Available online: https://www.science.org/doi/10.1126/science.abn1663 (accessed on 4 November 2024).
18. Bell, J.R.; Shephard, G. How aphids fly: Take-off, free flight and implications for short and long distance migration. *Agric. For. Entomol.* **2024**, 1–10. https://doi.org/10.1111/afe.12623
19. Nieminen, M.; Leskinen, M.; Helenius, J. Doppler radar detection of exceptional mass-migration of aphids into Finland. *Int. J. Biometeorol.* **2000**, *44*, 172–181. https://doi.org/10.1007/s004840000064
20. Parry, H.R. Cereal aphid movement: general principles and simulation modelling. *Mov. Ecol.* **2013**, *1*, 14. https://doi.org/10.1186/2051-3933-1-14
21. Crossley, M.S.; Lagos-Kutz, D.; Davis, T.S.; Eigenbrode, S.D.; Hartman, G.L.; Voegtlin, D.J.; Snyder, W.E. Precipitation change accentuates or reverses temperature effects on aphid dispersal. *Ecol. Appl.* **2022**, *32*, e2593. https://doi.org/10.1002/eap.2593.
22. Drake, V.A.; Reynolds, D.R. *Radar Entomology: Observing Insect Flight and Migration*; CABI Publishing: Wallingford, UK, 2010.

23. Morsello, S.C.; Groves, R.L.; Nault, B.A.; Kennedy, G.G. Temperature and Precipitation Affect Seasonal Patterns of Dispersing Tobacco Thrips, Frankliniella fusca, and Onion Thrips, Thrips tabaci (Thysanoptera: Thripidae) Caught on Sticky Traps. *Environ. Entomol.* **2008**, *37*, 79–86.
24. Pasek, J.E. 30. Influence of Wind and Windbreaks on Local Dispersal of Insects. *Agric. Ecosyst. Environ.* **1988**, *22*, 539–554.
25. Reynolds, A.M.; Reynolds, D.R. Aphid aerial density profiles are consistent with turbulent advection amplifying flight behaviours: Abandoning the epithet "passive". *Proc. R. Soc. B Biol. Sci.* **2009**, *276*, 137–143. https://doi.org/10.1098/rspb.2008.0880
26. Blazquez-Cabrera, S.; Bodin, Ö.; Saura, S. Indicators of the impacts of habitat loss on connectivity and related conservation priorities: Do they change when habitat patches are defined at different scales? *Ecol. Indic.* **2014**, *45*, 704–716. https://doi.org/10.1016/j.ecolind.2014.05.028
27. Mancini, F.; Hodgson, J.A.; Isaac, N.J.B. Co-designing an Indicator of Habitat Connectivity for England. *Front. Ecol. Evol.* **2022**, *10*, 892987. https://doi.org/10.3389/fevo.2022.892987
28. Platts, P.J.; Mason, S.C.; Palmer, G.; Hill, J.K.; Oliver, T.H.; Powney, G.D.; Fox, R.; Thomas, C.D. Habitat availability explains variation in climate-driven range shifts across multiple taxonomic groups. *Sci. Rep.* **2019**, *9*, 15039. https://doi.org/10.1038/s41598-019-51582-2
29. Proestos, Y.; Christophides, G.K.; Ergüler, K.; Tanarhte, M.; Waldock, J.; Lelieveld, J. Present and future projections of habitat suitability of the Asian tiger mosquito, a vector of viral pathogens, from global climate simulation. *Philos. Trans. R. Soc. B Biol. Sci.* **2015**, *370*, 1–16. https://doi.org/10.1098/rstb.2013.0554
30. Trakhtenbrot, A.; Nathan, R.; Perry, G.; Richardson, D.M. The importance of long-distance dispersal in biodiversity conservation. *Divers. Distrib.* **2005**, *11*, 173–181. https://doi.org/10.1111/j.1366-9516.2005.00156.x
31. Alzate, A.; Onstein, R.E. Understanding the relationship between dispersal and range size. *Ecol. Lett.* **2022**, *25*, 2303–2323. https://doi.org/10.1111/ele.14089
32. Liu, B.R. Biphasic range expansions with short- and long-distance dispersal. *Theor. Ecol.* **2021**, *14*, 409–427. https://doi.org/10.1007/s12080-021-00505-x
33. Marco, D.E.; Montemurro, M.A.; Cannas, S.A. Comparing short and long-distance dispersal: modelling and field case studies. *Ecography* **2011**, *34*, 671–682. Available online: https://www.jstor.org/stable/41239430 (accessed on 4 November 2024).
34. Mitchell, Z. Dragonfly Locomotion: Ecology, Form and Function. Ph.D. Thesis, University of Leeds, Leeds, UK, 2018.
35. Flockhart, D.T.T.; Fitzgerald, B.; Brower, L.P.; Derbyshire, R.; Altizer, S.; Hobson, K.A.; Wassenaar, L.I.; Norris, D.R. Migration distance as a selective episode for wing morphology in a migratory insect. *Mov. Ecol.* **2017**, *5*, 7. https://doi.org/10.1186/s40462-017-0098-9
36. Gao, B.; Hedlund, J.; Reynolds, D.R.; Zhai, B.; Hu, G.; Chapman, J.W. The 'migratory connectivity' concept, and its applicability to insect migrants. *Mov. Ecol.* **2020**, *8*, 48. https://doi.org/10.1186/s40462-020-00235-5
37. Jordano, P. What is long-distance dispersal? And a taxonomy of dispersal events. *J. Ecol.* **2017**, *105*, 75–84. https://doi.org/10.1111/1365-2745.12690
38. Chilson, P.B.; Bridge, E.; Frick, W.F.; Chapman, J.W.; Kelly, J.F. Radar aeroecology: Exploring the movements of aerial fauna through radio-wave remote sensing. *Biol. Lett.* **2012**, *8*, 698–701. https://doi.org/10.1098/rsbl.2012.0384.
39. Diehl, R.H. The airspace is habitat. *Trends Ecol. Evol.* **2013**, *28*, 377–379. https://doi.org/10.1016/j.tree.2013.02.015.
40. Braderic, M. On the Radar: Weather, Bird Migration and Aeroconservation over the North Sea. Ph.D. Thesis. Institute for Biodiversity and Ecosystem Dynamics, Amsterdam, The Netherlands, 2022.
41. Horton, K.G.; Van Doren, B.M.; Stepanian, P.M.; Farnsworth, A.; Kelly, J.F. Where in the air? Aerial habitat use of nocturnally migrating birds. *Biol. Lett.* **2016**, *12*, 20160591. https://doi.org/10.1098/rsbl.2016.0591
42. Aralimarad, P.; Reynolds, A.M.; Lim, K.S.; Reynolds, D.R.; Chapman, J.W. Flight altitude selection increases orientation performance in high-flying nocturnal insect migrants. *Anim. Behav.* **2011**, *82*, 1221–1225. https://doi.org/10.1016/j.anbehav.2011.09.013
43. Mateos-Rodríguez, M.; Liechti, F. How do diurnal long-distance migrants select flight altitude in relation to wind? *Behav. Ecol.* **2012**, *23*, 403–409. https://doi.org/10.1093/beheco/arr204
44. Wood, C.R.; Reynolds, D.R.; Wells, P.M.; Barlow, J.F.; Woiwod, I.P.; Chapman, J.W. Flight periodicity and the vertical distribution of high-altitude moth migration over southern Britain. *Bull. Entomol. Res.* **2009**, *99*, 525–535. https://doi.org/10.1017/S0007485308006548
45. Srygley, R.B.; Dudley, R. Optimal strategies for insects migrating in the flight boundary layer: Mechanisms and consequences. *Integr. Comp. Biol.* **2008**, *48*, 119–133. https://doi.org/10.1093/icb/icn011
46. Reynolds, D.R.; Smith, A.D.; Chapman, J.W. A radar study of emigratory flight and layer formation by insects at dawn over southern Britain. *Bull. Entomol. Res.* **2008**, *98*, 35–52. https://doi.org/10.1017/S0007485307005470
47. Wainwright, C.E.; Stepanian, P.M.; Reynolds, D.R.; Reynolds, A.M. The movement of small insects in the convective boundary layer: Linking patterns to processes. *Sci. Rep.* **2017**, *7*, 5438. https://doi.org/10.1038/s41598-017-04503-0
48. Neely, R.; Bennett, L.; Blyth, A.; Collier, C.; Dufton, D.; Groves, J.; Walker, D.; Walden, C.; Bradford, J.; Brooks, B.; et al. The NCAS mobile dual-polarisation Doppler X-band weather radar (NXPol). *Atmos. Meas. Tech.* **2018**, *11*, 6481–6494. https://doi.org/10.5194/amt-11-6481-2018.
49. Anjita, N.A.; Indu, J. Leveraging weather radars for desert locust monitoring. *Remote Sens. Appl. Soc. Environ.* **2023**, *31*, 100983. https://doi.org/10.1016/j.rsase.2023.100983

50. Shamoun-Baranes, J.; Bauer, S.; Chapman, J.W.; Desmet, P.; Dokter, A.M.; Farnsworth, A.; van Gasteren, H.; Haest, B.; Koistinen, J.; Kranstauber, B.; et al. Meteorological Data Policies Needed to Support Biodiversity Monitoring with Weather Radar. *Bull. Am. Meteorol. Soc.* **2022**, *103*, E1234–E1242. https://doi.org/10.1175/BAMS-D-21-0196.1
51. Tielens, E.K.; Cimprich, P.M.; Clark, B.A.; Dipilla, A.M.; Kelly, J.F.; Mirkovic, D.; Strand, A.I.; Zhai, M.; Stepanian, P.M. Nocturnal city lighting elicits a macroscale response from an insect outbreak population. *Biol. Lett.* **2021**, *17*, 20200808. https://doi.org/10.1098/rsbl.2020.0808
52. Chapman, J.W.; Reynolds, D.R.; Smith, A.D. Vertical-Looking Radar: A New Tool for Monitoring High-Altitude Insect Migration. *BioScience* **2003**, *53*, 503–511. https://doi.org/10.1641/0006-3568(2003)053[0503:VRANTF]2.0.CO;2
53. Stepanian, P.M.; Horton, K.G.; Melnikov, V.M.; Zrnić, D.S.; Gauthreaux, S.A. Dual-polarization radar products for biological applications. *Ecosphere* **2016**, *7*, e01539. https://doi.org/10.1002/ecs2.1539
54. Horn, J.W.; Kunz, T.H. Analyzing NEXRAD doppler radar images to assess nightly dispersal patterns and population trends in Brazilian free-tailed bats (Tadarida brasiliensis). *Integr. Comp. Biol.* **2007**, *48*, 24–39. https://doi.org/10.1093/icb/icn051
55. Wainwright, C.E.; Volponi, S.N.; Stepanian, P.M.; Reynolds, D.R.; Richter, D.H. Using cloud radar to investigate the effect of rainfall on migratory insect flight. Methods *Ecol. Evol.* **2022**, *14*, 655–668. https://doi.org/10.1111/2041-210X.14023
56. Alerstam, T.; Chapman, J.W.; Bäckman, J.; Smith, A.D.; Karlsson, H.; Nilsson, C.; Reynolds, D.R.; Klaassen RH, G.; Hill, J.K. Convergent patterns of long-distance nocturnal migration in noctuid moths and passerine birds. *Proc. R. Soc. B Biol. Sci.* **2011**, *278*, 3074–3080. https://doi.org/10.1098/rspb.2011.0058
57. Gürbüz, S.Z.; Reynolds, D.R.; Koistinen, J.; Liechti, F.; Leijnse, H.; Shamoun-Baranes, J.; Dokter, A.M.; Kelly, J.; Chapman, J.W. Exploring the skies: Technological challenges in radar aeroecology. In Proceedings of the IEEE National Radar Conference, Arlington, VA, USA, 10–15 May 2015; pp. 817–822. https://doi.org/10.1109/RADAR.2015.7131108
58. Hüppop, O.; Ciach, M.; Diehl, R.; Reynolds, D.R.; Stepanian, P.M.; Menz MH, M. Perspectives and challenges for the use of radar in biological conservation. *Ecography* **2019**, *42*, 912–930. https://doi.org/10.1111/ecog.04063
59. Wu, Q.L.; Westbrook, J.K.; Hu, G.; Lu, M.H.; Liu, W.C.; Sword, G.A.; Zhai, B.P. Multiscale analyses on a massive immigration process of Sogatella furcifera (Horváth) in south-central China: influences of synoptic-scale meteorological conditions and topography. *Int. J. Biometeorol.* **2018**, *62*, 1389–1406. https://doi.org/10.1007/s00484-018-1538-y
60. Chilson, P.B.; Frick, W.F.; Kelly, J.F.; Liechti, F. Aeroecology; Springer Link: Berlin/Heidelberg, Germany, 2017.
61. Kelly, J.F.; Stepanian, P.M. Radar aeroecology. *Remote Sens.* **2020**, *12*, 277–309. https://doi.org/10.3390/rs12111768
62. Kunz, T.H.; Gauthreaux, S.A.; Hristov, N.I.; Horn, J.W.; Jones, G.; Kalko, E.K.V.; Larkin, R.P.; McCracken, G.F.; Swartz, S.M.; Srygley, R.B.; et al. Aeroecology: Probing and modeling the aerosphere. *Integr. Comp. Biol.* **2008**, *48*, 1–11. https://doi.org/10.1093/icb/icn037
63. Aubry, S.; Labaune, C.; Magnin, F.; Roche, P.; Kiss, L. Active and passive dispersal of an invading land snail in Mediterranean France. *J. Anim. Ecol.* **2006**, *75*, 802–813. https://doi.org/10.1111/j.1365-2656.2006.01100.x
64. Drew, C.A.; Eggleston, D.B. Currents, landscape structure, and recruitment success along a passive-active dispersal gradient. *Landsc. Ecol.* **2006**, *21*, 917–931. https://doi.org/10.1007/s10980-005-5568-6
65. Wang, J.; Huang, Y.; Huang, L.; Dong, Y.; Huang, W.; Ma, H.; Zhang, H.; Zhang, X.; Chen, X.; Xu, Y. Migration risk of fall armyworm (Spodoptera frugiperda) from North Africa to Southern Europe. *Front. Plant Sci.* **2023**, *14*, 1141470. https://doi.org/10.3389/fpls.2023.1141470
66. Chen, H.; Wang, Y.; Huang, L.; Xu, C.F.; Li, J.H.; Wang, F.Y.; Cheng, W.; Gao, B.Y.; Chapman, J.W.; Hu, G. Flight Capability and the Low Temperature Threshold of a Chinese Field Population of the Fall Armyworm Spodoptera frugiperda. *Insects* **2022**, *13*, 422. https://doi.org/10.3390/insects13050422
67. Wu, M.F.; Qi, G.J.; Chen, H.; Ma, J.; Liu, J.; Jiang, Y.Y.; Lee, G.S.; Otuka, A.; Hu, G. Overseas immigration of fall armyworm, Spodoptera frugiperda (Lepidoptera: Noctuidae), invading Korea and Japan in 2019. Insect Sci. **2022**, *29*, 505–520. https://doi.org/10.1111/1744-7917.12940
68. Hodgson, J.A.; Randle, Z.; Shortall, C.R.; Oliver, T.H. Where and why are species' range shifts hampered by unsuitable landscapes? *Glob. Chang. Biol.* **2022**, *28*, 4765–4774. https://doi.org/10.1111/gcb.16220
69. Rubenstein, M.A.; Weiskopf, S.R.; Bertrand, R.; Carter, S.L.; Comte, L.; Eaton, M.J.; Johnson, C.G.; Lenoir, J.; Lynch, A.J.; Miller, B.W.; et al. Climate change and the global redistribution of biodiversity: substantial variation in empirical support for expected range shifts. *Environ. Evid.* **2023**, *12*, 7. https://doi.org/10.1186/s13750-023-00296-0
70. Drury, D.W.; Whitesell, M.E.; Wade, M.J. The effects of temperature, relative humidity, light, and resource quality on flight initiation in the red flour beetle, Tribolium castaneum. *Entomol. Exp. Appl.* **2016**, *158*, 269–274.
71. Hart, A.G.; Hesselberg, T.; Nesbit, R.; Goodenough, A.E. The spatial distribution and environmental triggers of ant mating flights: using citizen-science data to reveal national patterns. *Ecography* **2018**, *41*, 877–888. https://doi.org/10.1111/ecog.03140
72. Venter, G.J.; Boikanyo SN, B.; De Beer, C.J. The influence of temperature and humidity on the flight activity of Culicoides imicola both under laboratory and field conditions. *Parasites Vectors* **2019**, *12*, 4. https://doi.org/10.1186/s13071-018-3272-z
73. ECMWF. *IFS Documentation CY48R1*; ECMWF: Reading, UK, 2023.
74. Morton, R.D.; Marston, C.G.; O'Neil, A.W.; Rowland, C.S. *Land Cover Map 2017 (1km Classified Pixels, GB)*; UK Centre for Ecology & Hydrology: Lancaster, UK, 2020.
75. Boomsma, J.J.; Leusink, A. Weather Conditions during Nuptial Flights of Four European Ant Species. *Oecologia* **1981**, *50*, 236–241.

76. Staab, M.; Kleineidam, C. Initiation of swarming behavior and synchronization of mating flights in the leaf-cutting ant Atta vollenweideri FOREL, 1893 (Hymenoptera: Formicidae). *Myrmecol. News* **2013**, *19*, 93–102.
77. Knop, E.; Grimm, M.L.; Korner-Nievergelt, F.; Schmid, B.; Liechti, F. Patterns of high-flying insect abundance are shaped by landscape type and abiotic conditions. *Sci. Rep.* **2023**, *13*, 15114. https://doi.org/10.1038/s41598-023-42212-z
78. QGIS.org. QGIS Geographic Information System. QGIS Association, 2014. Available online: https://www.qgis.org (accessed on 4 November 2024).
79. Thuiller, W.; Georges, D.; Gueguen, M.; Engler, R.; Breiner, F.; Lafourcade, B.; Patin, R. biomod2: Ensemble Platform for Species Distribution Modeling (R 4.2-2), 2023. Available online: https://CRAN.R-project.org/package=biomod2 (accessed on 4 November 2024).
80. Kilambi, A.; Fabry, F.; Meunier, V. A simple and effective method for separating meteorological from nonmeteorological targets using dual-polarization data. *J. Atmos. Ocean. Technol.* **2018**, *35*, 1415–1424. https://doi.org/10.1175/JTECH-D-17-0175.1
81. Helmus, J.J.; Collis, S.M. The Python ARM Radar Toolkit (Py-ART), a Library for Working with Weather Radar Data in the Python Programming Language. *J. Open Res. Softw.* **2016**, *4*, 25. https://doi.org/10.5334/jors.119
82. Lukach, M.; Dally, T.; Evans, W.; Hassall, C.; Duncan, E.J.; Bennett, L.; Addison, F.I.; Kunin, W.E.; Chapman, J.W.; Neely, R.R. The development of an unsupervised hierarchical clustering analysis of dual-polarization weather surveillance radar observations to assess nocturnal insect abundance and diversity. *Remote Sens. Ecol. Conserv.* **2022**, *8*, 698–716. https://doi.org/10.1002/rse2.270
83. Allouche, O.; Tsoar, A.; Kadmon, R. Assessing the accuracy of species distribution models: Prevalence, kappa and the true skill statistic (TSS). *J. Appl. Ecol.* **2006**, *43*, 1223–1232. https://doi.org/10.1111/j.1365-2664.2006.01214.x
84. Hanczar, B.; Hua, J.; Sima, C.; Weinstein, J.; Bittner, M.; Dougherty, E.R. Small-sample precision of ROC-related estimates. *Bioinformatics* **2010**, *26*, 822–830. https://doi.org/10.1093/bioinformatics/btq037
85. Lobo, J.M.; Jiménez-valverde, A.; Real, R. AUC: A misleading measure of the performance of predictive distribution models. *Glob. Ecol. Biogeogr.* **2008**, *17*, 145–151. https://doi.org/10.1111/j.1466-8238.2007.00358.x
86. Wickham, H. ggplot2: Elegant Graphics for Data Analysis (4.3.3); Springer: New York, NY, USA, 2016. Available online: https://ggplot2.tidyverse.org (accessed on 4 November 2024).
87. R Core Team. *R: A Language and Environment for Statistical Computing (4.2.2)*; R Foundation for Statistical Computing: Vienna, Austria, 2022.
88. Sillero, N.; Arenas-Castro, S.; Enriquez-Urzelai, U.; Vale, C.G.; Sousa-Guedes, D.; Martínez-Freiría, F.; Real, R.; Barbosa, A.M. Want to model a species niche? A step-by-step guideline on correlative ecological niche modelling. *Ecol. Model.* **2021**, *456*, 109671. https://doi.org/10.1016/j.ecolmodel.2021.109671
89. Sillero, N.; Barbosa, A.M. Common mistakes in ecological niche models. *Int. J. Geogr. Inf. Sci.* **2021**, *35*, 213–226. https://doi.org/10.1080/13658816.2020.1798968
90. Kautz, M.; Imron, M.A.; Dworschak, K.; Schopf, R. Dispersal variability and associated population-level consequences in tree-killing bark beetles. *Mov. Ecol.* **2015**, *4*, 9. https://doi.org/10.1186/s40462-016-0074-9
91. Koralewski, T.E.; Wang, H.-H.; Grant, W.E.; Brewer, M.J.; Elliott, N.C.; Westbrook, J.K. Modeling the dispersal of wind-borne pests: Sensitivity of infestation forecasts to uncertainty in parameterization of long-distance airborne dispersal. *Agric. For. Meteorol.* 2021, 301–302, 108357. https://doi.org/10.1016/j.agrformet.2021.108357
92. Mungee, M.; Lukach, M.; Shortall, C.; Bell, J.R.; Duncan, E.J.; Addison, F.; Brown, L.; Kunin, W.E.; Hassall, C.; Neely, R.R., III. Weather radar reveal spatio-temporal trends in aerial arthropod abundance at a national scale. **2024**, *In Review*.
93. Van Doren, B.M.; Horton, K.G. A continental system for forecasting bird migration. *Science* **2018**, *361*, 1115–1118. https://doi.org/10.6084/m9.figshare.6962810
94. Knight, S.M.; Pitman, G.M.; Flockhart DT, T.; Norris, D.R. Radio-tracking reveals how wind and temperature influence the pace of daytime insect migration. *Biol. Lett.* **2019**, *15*, 20190327. https://doi.org/10.1098/rsbl.2019.0327
95. Pretorius, I.; Schou, W.C.; Richardson, B.; Ross, S.D.; Withers, T.M.; Schmale Iii, D.G.; Strand, T.M. In the wind: Invasive species travel along predictable atmospheric pathways. *Ecol. Appl.* **2023**, *33*, e2806. https://doi.org/10.5281/zenodo.7324857
96. Chen, Y.; Aukema, B.H.; Seybold, S.J. The effects of weather on the flight of an invasive bark beetle, Pityophthorus juglandis. *Insects* **2020**, *11*, 156. https://doi.org/10.3390/insects11030156
97. Waldock, J.; Chandra, N.L.; Lelieveld, J.; Proestos, Y.; Michael, E.; Christophides, G.; Parham, P.E. The role of environmental variables on Aedes albopictus biology and chikungunya epidemiology. *Pathog. Glob. Health* **2013**, *107*, 224–241. https://doi.org/10.1179/2047773213Y.0000000100
98. Martini, X.; Stelinski, L.L. Influence of abiotic factors on flight initiation by Asian citrus psyllid (hemiptera: Liviidae). *Environ. Entomol.* **2017**, *46*, 369–375. https://doi.org/10.1093/ee/nvx039
99. Benton, T.G.; Bryant, D.M.; Cole, L.; Crick, H.Q.P. Linking agricultural practice to insect and bird populations: A historical study over three decades. *J. Appl. Ecol.* **2002**, *39*, 673–687. https://doi.org/10.1046/j.1365-2664.2002.00745.x
100. Outhwaite, C.L.; McCann, P.; Newbold, T. Agriculture and climate change are reshaping insect biodiversity worldwide. *Nature* **2022**, *605*, 97–102. https://doi.org/10.1038/s41586-022-04644-x
101. Ziesche, T.M.; Ordon, F.; Schliephake, E.; Will, T. Long-term data in agricultural landscapes indicate that insect decline promotes pests well adapted to environmental changes. *J. Pest Sci.* **2023**, *97*, 1281–1297. https://doi.org/10.1007/s10340-023-01698-2
102. Blumgart, D.; Botham, M.S.; Menéndez, R.; Bell, J.R. Moth declines are most severe in broadleaf woodlands despite a net gain in habitat availability. *Insect Conserv. Divers.* **2022**, *15*, 496–509. https://doi.org/10.1111/icad.12578

103. Jackson, D.L. *Guidance on the Interpretation of the Biodiversity Broad Habitat Classification (Terrestrial and Freshwater Types): Definitions and the Relationship with Other Classifications*; Joint Nature Conservation Committee: Peterborough, UK, 2000.
104. Henrys, P.A.; Jarvis, S.G. Integration of ground survey and remote sensing derived data: Producing robust indicators of habitat extent and condition. *Ecol. Evol.* **2019**, *9*, 8104–8112. https://doi.org/10.1002/ece3.5376
105. Jatau, P.; Melnikov, V.; Yu, T.-Y. Detecting Birds and Insects in the Atmosphere Using Machine Learning on NEXRAD Radar Echoes. *Environ. Sci. Proc.* **2021**, *8*, 48. https://doi.org/10.3390/ecas2021-10352
106. Nussbaumer, R.; Schmid, B.; Bauer, S.; Liechti, F. A gaussian mixture model to separate birds and insects in single-polarization weather radar data. *Remote Sens.* **2021**, *13*, 1989. https://doi.org/10.3390/rs13101989
107. Zaugg, S.; Saporta, G.; van Loon, E.; Schmaljohann, H.; Liechti, F. Automatic identification of bird targets with radar via patterns produced by wing flapping. *J. R. Soc. Interface* **2008**, *5*, 1041–1053. https://doi.org/10.1098/rsif.2007.1349
108. Baldini, L.; Gorgucci, E. Identification of the Melting Layer through Dual-Polarization Radar Measurements at Vertical Incidence. *J. Atmos. Ocean. Technol.* **2006**, *23*, 829–839. https://doi.org/10.1175/JTECH1884.1
109. Ryzhkov, A.; Krause, J. New Polarimetric Radar Algorithm for Melting-Layer Detection and Determination of Its Height. *J. Atmos. Ocean. Technol.* **2022**, *39*, 529–543. https://doi.org/10.1175/JTECH-D-21-0130.1
110. Rocchini, D.; Tordoni, E.; Marchetto, E.; Marcantonio, M.; Barbosa, A.M.; Bazzichetto, M.; Beierkuhnlein, C.; Castelnuovo, E.; Gatti, R.C.; Chiarucci, A.; et al. A quixotic view of spatial bias in modelling the distribution of species and their diversity. *NPJ Biodivers.* **2023**, *2*, 10. https://doi.org/10.1038/s44185-023-00014-6
111. Hao, Z.; Drake, V.A.; Taylor, J.R.; Warrant, E. Insect target classes discerned from entomological radar data. *Remote Sens.* **2020**, *12*, 673. https://doi.org/10.3390/rs12040673
112. Bell, J.R.; Aralimarad, P.; Lim, K.-S.; Chapman, J.W. Predicting Insect Migration Density and Speed in the Daytime Convective Boundary Layer. *PLoS ONE* **2013**, *8*, e54202. https://doi.org/10.1371/journal.pone.0054202
113. Drake, V.A.; Wang, H.K.; Harman, I.T. Insect monitoring radar: remote and network operation. *Comput. Electron. Agric.* **2002**, *35*, 77–94.
114. Adonyeva, N.V.; Menshanov, P.N.; Gruntenko, N. A link between atmospheric pressure and fertility of drosophila laboratory strains. *Insects* **2021**, *12*, 947. https://doi.org/10.3390/insects12100947
115. Guarneri, A.A.; Lazzari, C.; Diotaiuti, L.; Lorenzo, M.G. The effect of relative humidity on the behaviour and development of Triatoma brasiliensis. *Physiol. Entomol.* **2002**, *27*, 142–147. https://doi.org/10.1046/j.1365-3032.2002.00279.x
116. Norhisham, A.R.; Abood, F.; Rita, M.; Rehman Hakeem, K. Effect of humidity on egg hatchability and reproductive biology of the bamboo borer (Dinoderus minutus Fabricius). *SpringerPlus* **2013**, *2*, 1–6.
117. Solbreck, C.; Knape, J.; Förare, J. Role of weather and other factors in the dynamics of a low-density insect population. *Ecol. Evol.* **2022**, *12*, e9261. https://doi.org/10.1002/ece3.9261
118. Bennett, L. *NCAS Mobile X-Band Radar Scan Data from 1st November 2016 to 4th June 2018 Deployed on Long-Term Observations at the Chilbolton Facility for Atmospheric and Radio Research (CFARR), Hampshire, UK*; Centre for Environmental Data Analysis: Didcot, UK, 2020. https://doi.org/10.5285/ffc9ed384aea471dab35901cf62f70be.